APPLICATION OF THE WAVELET TRANSFORM FOR EMG M-WAVE PATTERN RECOGNITION

APPLICATION OF THE WAVELET TRANSFORM FOR EMG M-WAVE PATTERN RECOGNITION

By

JILLIAN SALVADOR, B.ENG.

A Thesis

Submitted to the School of Graduate Studies

in Partial Fulfillment of the Requirements

for the Degree

Master of Applied Science

McMaster University

MASTER OF APPLIED SCIENCE McMASTER UNIVERSITY

(Electrical Engineering) Hamilton, Ontario

TITLE: Application of the Wavelet Transform for EMG M-Wave Pattern Recognition

AUTHOR: Jillian Salvador, B.Eng. (McMaster University)

SUPERVISOR: Dr. H. de Bruin

NUMBER OF PAGES: xi, 102

ABSTRACT

An investigation as to the appropriateness of the wavelet transform for surface electromyography (EMG) M-wave pattern recognition is described. The M-waves are obtained by stimulating the median nerve at the wrist to activate the motor units. Surface electrodes and a graded stimulus amplitude are used. The resulting M-waves are classified using both wavelet vectors and the traditional power spectral coefficients as features sets in the pattern recognition scheme. A novel system was developed to obtain M-wave collections from subjects in the laboratory and to perform both real-time and off-line analysis.

The results obtained from the left and right thenar muscles of 4 healthy females and 2 healthy males are presented. These results are further analyzed offline to determine the effects of a changing discriminatory threshold for both wavelet and power spectral pattern recognition techniques. In addition, intra-class and inter-class Euclidean distances are shown for the set of unique M-waves derived from using the different feature sets. A time-invariant wavelet transform is implemented to improve classification by eliminating errors due to latency shifts.

The results show that the number of unique M-waves obtained using wavelet features is less sensitive to a variation in discriminatory threshold. It may be concluded that a wavelet based feature set shows slight improvement in M-wave pattern classification. The time-invariant wavelet offers further accuracy.

ACKNOWLEDGEMENTS

I would like to thank Dr. H. de Bruin for his assistance and support throughout the development of this thesis. His enthusiasm was contagious and contributed to making my experience at McMaster an enjoyable one. I would also like to express an appreciation for the advice of Dr. A.J. McComas and Dr. T. Davidson. Special recognition should be given to Cheryl Gies for her friendly assistance with all administrative matters. Finally, I would like to thank my friends and family, especially my parents, for their constant love and encouragement.

TABLE OF CONTENTS

LIST OF FIGURES viii

LIST OF TABLES x

LIST OF ABBREVIATIONS xi

CHAPTER 1 1

1.1 Introduction 1

1.2 Summary of Chapters 2

CHAPTER 2 3

2.1 Introduction 3

2.2 Skeletal Muscle 3

2.3 Surface Stimulation and Recording 6

2.4 Disorders of the Motor Unit 10

2.5 Motor Unit Number Estimation 11

2.6 Downfalls of the McComas Technique 13

2.7 Improvements to the McComas Technique 14

2.8 Summary 17

CHAPTER 3 19

3.1 Introduction 19

3.2 Power Spectral Features 20

3.3 Short-Time Fourier Transform 23

3.4 Wavelet Analysis 24

3.5 Time-Invariant Wavelet Analysis 29

CHAPTER 4 32

4.1 Introduction 32

4.1.1 Subject Set-up 32

4.1.2 Electrodes 33

4.1.3 EMG Amplifier 33

4.1.4 Stimulator 36

4.2 Software 36

4.2.1 System Parameters 37

4.2.2 Synch AIAO 41

4.2.3 Signal Processing 43

4.2.3.1 Differential 60 Hz Noise Reduction 44

4.2.3.2 Stimulus Artifact Removal 46

4.2.3.3 Response Rejection 48

4.2.3.4 Signal Feature Extraction 48

4.2.3.5 Fourier Transforms 49

4.2.3.6 Wavelet Transforms 50

4.2.4 Experimental Protocol 50

4.2.4.1 MEP Collection 51

4.2.4.2 Sub-maximal Collection 53

4.2.5 M-Wave Classification 55

4.2.6 Program Termination 56

4.2.7 Storage 58

CHAPTER 5 59

5.1 Introduction 59

5.2 Evaluating and Comparing M-wave Pattern Recognition Schemes 59

5.3 Motivation for a Characteristic Discriminator 60

5.4 Threshold Determination 63

5.5 Choice of the Wavelet Transform 66

5.6 Comparison of Power Spectral and Wavelet Features 70

5.7 Intra- and Inter-Class Distances 79

5.8 Motor Unit Number Estimates 83

5.9 Alternate Wavelets 85

5.10 Time Invariant Wavelet 94

CHAPTER 6 99

6.1 Conclusions 99

6.2 Future Research 101

REFERENCES 102

LIST OF FIGURES

2.1 The Motor Unit 5

2.2 Cross-section of a nerve trunk 8

2.3 Probability of motor unit firing 15

3.1 Daubechies 5 wavelet function and filter representation 27

3.2 Dyadic wavelet decomposition 28

3.3 Shift-invariant wavelet decomposition 31

4.1 Experimental instrumentation 34

4.2 Hardware overview 35

4.3 LabVIEW program front panel 38

4.4 Software flowchart 39

4.5 Response classification flowchart 40

4.6 Raw data recording 42

4.7 Signal processing of raw data 45

4.8 Maximum evoked potential window in LabVIEW program 52

4.9 Composite response 57

5.1 M-wave template number for 3 subjects over varying threshold 65

5.2 Daubechies family of mother wavelets 67

5.3 Power spectral density for subject A 69

5.4 Variation in M-wave number with threshold for one subject 72

5.5 Average M-wave number for varying thresholds 73

5.6 Average number of distinct M-waves greater than 10 74

5.7 Threshold sensitivity for average number of distinct M-waves.................................76

5.8 Index range for M-wave number within 20% of maximum number...........................80

5.9 Intra-class and inter-class Euclidean distance for one subject....................................81

5.10 Average number of distinct M-waves using db5 and db4 wavelets 87

5.11 Average number of distinct M-waves using db5 and Haar wavelets.........................89

5.12 Intra-class and inter-class Euclidean distance using Haar wavelet............................90

5.13 Power spectral density for subject B...91

5.14 Average number of distinct M-waves using A3/D3 and A4/D4 wavelet vectors......92

5.15 Latency shifting 95

5.16 Intra-class and inter-class Euclidean distance using shift-invariant wavelet.............96

LIST OF TABLES

5.1 Deviations from maximum M-wave number for index deviations 77

5.2 Distance between individual and average characteristic thresholds 78

5.3 Average variations in M-wave number with threshold 79

5.4 Thenar MUNEs for 6 subjects 83

5.5 Summary of thenar MUNEs in recent studies 85

LIST OF ABBREVIATIONS

AP = Action Potential

CR = Composite Response (M-Waves)

DWT = Discrete Wavelet Transform

EMG = Electromyography

MEP = Maximum Evoked Potential

MN = Motor Neuron

MSWR = Multi-Scale Wavelet Representation

MU = Motor Unit

MUAP = Motor Unit Action Potential

STFT = Short-Time Fourier Transform

CHAPTER 1
INTRODUCTION

1.1 Introduction

The smallest functional unit of skeletal muscle contraction is the motor unit (MU), consisting of the motor neuron (MN) and the muscle fibres innervated by it. Muscle contraction occurs with the asynchronized recruitment of individual MUs. Additionally, MU excitation can occur through the application of an electromagnetic stimulus. In the study of neuromuscular disease, the number of functional MUs gives relevant information concerning the progression of the disease. Moreover, MU number is important for diagnosis, monitoring effects of treatments, and in research studies such as age related changes.

In the past, different motor unit number estimation (MUNE) techniques have been developed. Most of these techniques require some form of pattern recognition, whether automated or manual, to extract unique M-wave templates from recorded evoked muscle responses. In automated pattern recognition, either power spectral coefficients or time-based measure were used as the features in the classification. These feature sets are not optimal and their inherent drawbacks affect the accuracy of the MUNE.

This thesis investigates the use of different feature sets for M-wave pattern recognition. Specifically, the applicability of the wavelet transform to M-wave classification is examined. In addition, a novel data collection computer interface was designed to record up to 20 unique M-waves per subject. This interface was equipped to perform real-time M-wave pattern recognition with both power spectral and wavelet feature sets. The system and classification approaches were developed and tested using the thenar muscles of a number of subjects. This necessitated the development of noise reduction algorithms to remove stimulus artifact and power line noise. Moreover, post-processing algorithms are applied to further investigate the various aspects of the wavelet transform. The results are compared with results in the literature obtained using alternative MUNE techniques.

1.2 Summary of Chapters

The following chapter describes the physiology of the MU, detailing its anatomy and the manner in which its electrical properties may be measured. The mathematical background for the different feature extractors used in this thesis is given in Chapter 3. Chapter 4 describes both the hardware and software designed for this research. Algorithms for M-wave pattern classification are also presented. In Chapter 5, the use of different feature sets for M-wave classification is thoroughly examined. The results for the left and right thenar muscles of 6 subjects are presented. Lastly, Chapter 6 summarizes the results obtained in this work and gives the direction for future research.

CHAPTER 2
BACKGROUND

2.1 Introduction

The following chapter outlines the physiological and anatomical background necessary for a full understanding of the work presented in this thesis. First, a detailed look at the properties of skeletal muscle, including the associated motor nerves, provides a background for motor unit number estimation (MUNE). Following, the progression of MUNE techniques and their inherent problems gives motivation for the research topic discussed in the remainder of this thesis.

2.2 Skeletal Muscle

The following outlines the electrophysiology of human skeletal muscle. A more detailed description may be found in references such as Guyton and Hall (2000).

Skeletal muscle is comprised of numerous fibres ranging in diameter from 10 to 80 micrometers that stretch the entire length of the muscle. Each fibre contains specialized intracellular components to facilitate muscle contraction and is innervated by a single nerve ending located near its center. The term motor unit (MU) is used to collectively describe the motor neuron (MN), whose cell body is located in the spinal column, a motor axon and its terminal branches, and the muscle fibres which the terminal branches innervate. The MU is the smallest functional unit of contraction in the human skeletal muscular system. A MU is depicted in Figure 2.1. As seen in this figure the motor axon is protected by a myelin sheath. These cells serve to insulate the conducting axon thus increasing the velocity of the electrical transmission along the nerve as discussed later. The MU size refers to the number and type of muscle fibres innervated by that MN. A given muscle may have a few to several hundred MUs of varying size. Feinstein et. al. (1955) used cadaveric studies to develop a database for the number of MUs in different human muscles. The range was large, with the thenar muscle found to have 203 MUs, while estimates for muscles such as the platysma (1096) and anterior tibalis (445) were much higher. The size of a MU correlates to the contribution of that MU to a muscle contraction. Thus, larger MUs will have a greater contribution to a skeletal muscle contraction than smaller units.

The event responsible for initiating muscle contraction is the action potential (AP). Both nerve and muscle cells are excitable. That is, a potential difference exists between the intra-cellular and extra-cellular media, and changes in this potential can result in an electrical signal that propagates along the cellular membrane. A MN in its resting state typically has a potential difference of -70mV across its cellular membrane. This potential difference is due to stationary intra-cellular anions and is maintained at equilibrium through selective membrane permeability to the positive ions potassium (K^+) and sodium (Na^+). An AP begins in the MN with a localized depolarization of the cellular membrane. This results in increased membrane permeability to Na^+ causing Na^+ to enter and the cell potential to increase and upon reaching a characteristic threshold level, becoming a positive feedback system. At this threshold, a mass influx of Na^+ results in the generation of an AP. An AP is an all-or-nothing event in that it occurs with

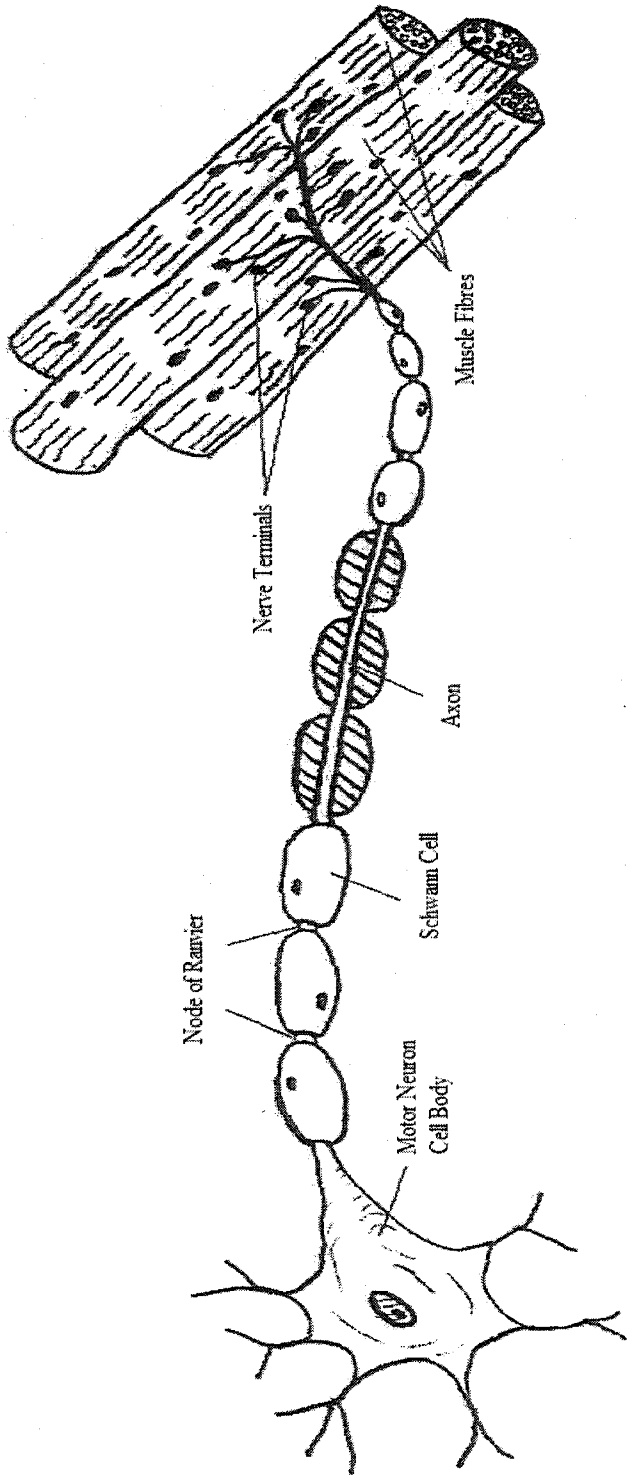

Figure 2.1. The motor unit (Orsi, 2000)

certainty once the threshold value is reached but otherwise does not occur. When the threshold value is reached and an AP is generated the nerve is said to have "fired". APs are generated in muscle fibres as well as in nerve fibres, using the same mechanism.

In natural, voluntary muscle contraction input from the brain and spinal cord of the central nervous system causes an AP to be generated in the MN of a MU. This AP propagates down the motor nerve axon, through the terminal branches and across the synaptic junctions to the muscle fibres of the motor unit. The firing of the muscle fibres creates a short contraction called a "twitch". Smooth, continuous contraction of the muscle occurs when the individual motor units are fired asynchronously and the resulting twitches are summed.

The location where the motor axon branches enter the muscle is termed the end plate zone and for most muscles is situated at the center of the muscle known as the muscle belly. An important anatomical property is that the muscle fibres of a given MU are not all adjacent. Instead, the muscle fibres innervated by one MN are overlapped with fibres of other MUs. Thus, the terminal branches of the MN are spatially dispersed through the end plate zone.

2.3 Surface Stimulation and Recording

The discussion to this point has described muscle contraction initiated voluntarily. In experimental situations it is difficult for an individual to control and maintain the force of a muscle contraction so quantitative measures can be recorded and reproduced. There are two methods to electrically stimulate a muscle contraction overriding conscious commands and enabling sufficient control and repeatability for experimental purposes. These are through extra-cellular surface stimulation or intra-cellular stimulation via a micro-electrode. The former approach is applicable to this thesis and will be discussed here.

The peripheral nervous system is structured such that MN fibres are bundled together with afferent sensory fibres in a nerve trunk. The nerve trunk is surrounded by a tough layer of high impedance connective tissue called the epineurium as shown in Figure 2.2. Surrounding the nerve trunk is a bath of body fluids that acts as a volume conductor through which an electric field can penetrate.

When two electrodes placed on the surface of the skin are supplied with a voltage difference, an electric field is generated and penetrates through the skin and into the body tissues. The electric field diminishes as the distance into the body away from the skin surface increases. However, the field establishes a potential difference and causes ion movement in the extra-cellular fluids. If the electric field is strong enough at the point where a nerve trunk is located, the field will penetrate the high impedance epineurium. The ions in the extra-cellular fluid within the nerve trunk will then experience a force causing their movement. This ion movement will result in a local depolarization of the nerve fibres in the region. This depolarization will only occur at the nodes of Ranvier in the myelinated motor nerve fibres (see Figure 2.1). If ion movement progresses to a great extent an AP in the affected nerve fibres will result. Moreover, if the electric field is increased it will penetrate deeper into the nerve trunk and additional fibres will fire.

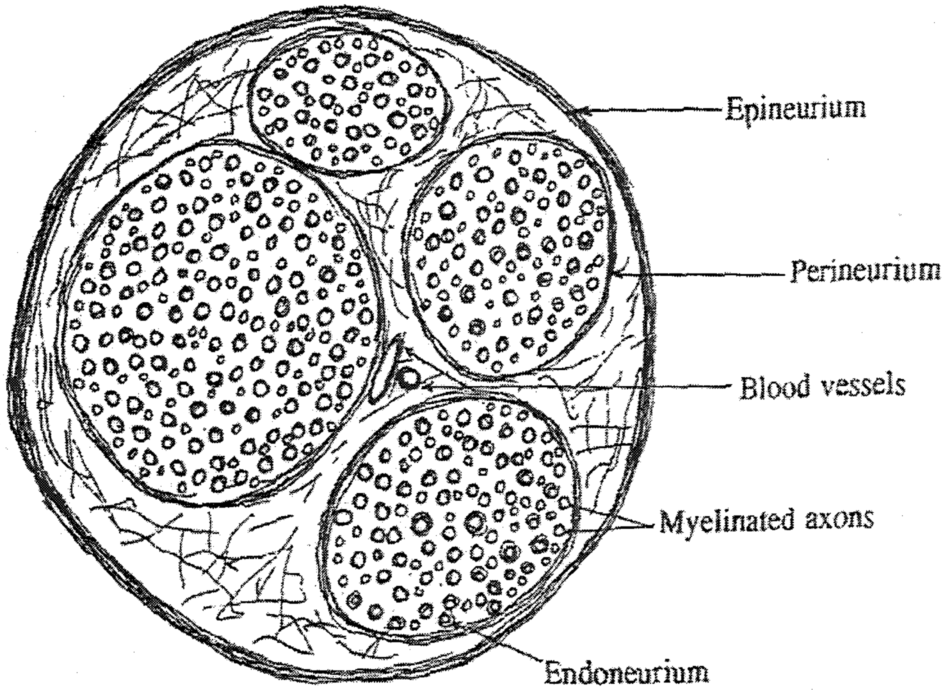

Figure 2.2. Cross-section of a nerve trunk containing myelinated and unmyelinated fibres (Guyton and Hall, 1996)

It is recognized that electric field depth alone does not determine the order in which MNs fire. The issue of preferential recruitment of MUs in surface stimulation has been one of dispute for many years. There is some debate as to whether the stimulus threshold of MN axons is only related to axon size or conduction velocity (Chan et al, 1998). Recent research has given evidence that recruitment depends on the depth of a fibre in a nerve bundle and other tissues as well as the fibre's axon size and the internal fibre state (Szlavik and deBruin, 1999). Axon size is deemed important because larger axons have longer distances between adjacent nodes of Ranvier and thus, a greater difference in external potential resulting from the same applied stimulus.

In this thesis, surface recordings of excited muscle fibre activities are examined. A recording can also be explained using a volume conductor. However, in contrast to stimulation, the source of electrical activity is the excited cell membrane, in this case a muscle fibre. When a nerve is stimulated to generate an AP, the potential travels along the axon to the muscle fibres it innervates, causing them to depolarize. The excited muscle fibre is a bioelectric source and can be approximated as a moving constant current source that delivers current to the extra-cellular bathing medium. This current produces a potential field in the volume conductor which can be measured by surface electrodes. Again, the potential field decreases with distance between the excited muscle fibre and the skin. When surface electrodes are placed over the muscle, the recording is the sum of all electrical activity occurring in the volume conductor as it affects potentials at the skin interface. Thus, the recording is comprised of electrical signals (APs) from all muscle fibres that are firing. As the muscle fibres are at varying distances from the recording electrode, the AP's are attenuated by varying amounts. Further, they are temporally dispersed because of the dispersion of synapses in the end plate regions. The sum of the temporally displaced APs is called an M-wave. When only one motor unit fires, the record is known as a motor unit action potential (MUAP). Therefore the shape of a MUAP is dependent on the spatial dispersion of MN terminal branches, the number of muscle fibres in the MU, their relative positions to the recording electrodes, and the sizes and distance of the two recording electrodes. If the recording electrode position remains unaltered the shape of the MUAP remains relatively constant, thus making MU pattern recognition possible.

2.4 Disorders of the Motor Unit

Muscle strength will be reduced should some of the MUs become diseased. When a neuropathy occurs, the problem in the MU is with the MN. This results in a loss of working MUs. Alternatively, the MU defect could be in the muscle fibre. This is a myopathy. Several diseases such as amyotrophic lateral sclerosis, spinal muscular atrophy and poliomyelitis are characterized by a loss of healthy motor units.

In the case of a neuropathy, healthy muscle fibres, still capable of contracting, have lost their MN. The nervous system compensates for this by re-innervating the healthy muscle fibres. The result is that the number of MUs is less but the number of working muscle fibres remains the same. Though the maximum muscle force is unaffected, the gradation of force is hindered because of the reduced MU population and the increased size of the MUs.

The health of the MUs can be used to distinguish between neuropathies and myopathies. Thus, the technique for accurately estimating the number of functional MUs and their characteristics presented in this thesis has value as both a research and a diagnostic tool. It can provide valuable information to aid in diagnosis or to monitor the progression of a muscle denervating disorder. Furthermore, MU numbers may demonstrate characteristics of a disease that are as of yet unsuspected by physicians.

2.5 Motor Unit Number Estimation

When stimulating electrodes placed over a nerve trunk are supplied with an electric pulse, some of the motor nerves are depolarized to produce an AP. As described above, this AP will propagate to the muscle fibres innervated by these motor nerves causing MUAPs. An additional recording electrode placed over the end plate region of the muscle that the stimulated nerve bundle controls measures the summation of all the evoked MUAPs. The data recorded by this electrode can be used to produce an estimate of the motor unit number in a process that is further outlined below.

The incremental motor unit number estimation (MUNE) technique originally proposed by McComas et. al. (1971) makes use of the patient instrumentation shown in Figure 4.1. In this technique an operator manually increases the stimulus to produce a set of evoked responses or M-waves known as the composite response (CR). The CR is a series of M-waves separated by discrete increments as illustrated in Figure 4.9. McComas assumed that each increment in the CR is the result of the addition of an MUAP due to the excitation of one more MN with the slight increase in stimulus. The maximum evoked potential (MEP) occurs when the stimulus pulse amplitude is increased so that all of the motor units within the muscle are firing. The MEP is a summation of the MUAPs from all of the motor units in the muscle.

McComas et. al. reasoned that if many individual summed MUAPs could be recorded and an average MUAP value calculated then an estimate for the number of motor units in a muscle is given by

$$\text{MUNE} = \frac{\text{MEP amplitude}}{\text{Average MUAP amplitude}}$$

In this manual technique, which used an oscilloscope and visual pattern recognition, the amplitude feature selected was the peak-to-peak amplitude of the M-wave. The average MUAP amplitude could be ascertained by performing successive subtractions of the M-waves in the CR to give the contributing MUAPs and averaging their amplitude feature. However, since MUAPs have different shapes and time durations, the MUAP amplitude features such as peak-to-peak amplitude do not add linearly. This can be compensated for by determining the average MUAP contribution to the M-wave amplitude feature. This contribution is simply the amplitude feature of the largest M-wave in the CR divided by the number of members in the CR. The assumption, therefore, is that the MUAPs in the total population of motor units in a muscle add in the same manner to form the MEP as they do in the much smaller sample that adds to form the CR.

This particular MUNE technique requires the stimulating and recording electrodes to have access to the nerve bundle and the associated muscle. Thus, muscles whose nerve supply is buried within body tissue, such as the biceps brachii are difficult to apply to this test. Muscles that are readily available for MUNE include the thenar, the hypothenar, the extensor digitorum brevis, the soleus, the first dorsal interosseus and the deltoid. The present research makes use of the thenar muscle as both its nerve bundle and its end plate region are readily accessibly for surface stimulation and recording. Moreover, there is a large research base concerning the properties of the human thenar muscle.

A typical thenar response for rectangular current pulse stimulation is shown in Figure 4.6 (A). This response consists of a stimulus artefact which is no longer rectangular but instead is exponentially decaying due to the filtering properties of the tissues and electrodes. Also present in the recorded response is a propagation delay due to the time required for the AP to travel along the axon and across the synaptic junction. Finally the response shows the M-wave which is the summated MUAPs.

2.6 Downfalls of the McComas Technique

Unfortunately, the incremental technique relies on several basic assumptions which limit the confidence level in MUNE achieved this way. The first underlying assumption of this technique is that each increment in the CR results from the recruitment of one additional MU. There are several conditions that may violate this assumption. First, there may be very small MUs, or MUs that are far beneath the surface recording electrodes that produce MUAPs on the same order of magnitude as the noise in the recording system. If this is the case it will be difficult, if not impossible, to determine these as increments in the CR. Thus, the number of MUAPs determined by the incremental technique will be low and the average MUAP value will be high. This results in an under-estimation of the MU number.

Secondly, it may be possible that two motor nerves have stimulation thresholds that are very close in value. Thus, the two MUs may repetitively fire together and separate MUAPs will not be discernable. Again, the number of MUAPs will be under-estimated causing an under-estimation of the MU number.

The most common point for criticism of the incremental technique is in relation to alternation. Alternation results from the fact that MU stimulation thresholds vary slightly over time. Thus, in the incremental technique there is a probability associated with the firing of a MU at specific stimuli amplitudes rather than a certainty of firing (Slawnych et. al., 1996). This probability curve is shown in Figure 2.3 (A). At stimulus level S_1, MU_1 will fire 0% of the time while at stimulus level S_2, MU_1 will fire 100% of the time. Alternation occurs when multiple MUs have overlapping probabilities of firing. For example in Figure 2.3 (A) at stimlus level S_3 both MU_3 and MU_4 have a probability of firing. Thus, there are three possible M-waves that may be seen at any given time at this stimlus level as shown if Figure 2.3 (B). When the number of MUs with overlapping probabilities of activation increases, the number of possible M-waves increases significantly. If these cases of alternation remain undetected the CR will contain too many increments resulting in an overestimate of the MUNE.

2.7 Improvements to the McComas Technique

McComas et. al., developed specific procedures for determining the MEP and the average MUAP which were carried out manually using a fully trained operator and storage oscilloscope. However, the semi-automation of these procedures by Ballantyne and Hansen (1974; 1975) improved reliability of the MU estimate. This system provided the operator with displays to aid in creating the CR. In addition the CR was stored in a computer as templates. The individual MUAPs could then be found by subtracting each template from the next largest. Ballantyne and Hansen also proposed ranking M-wave size by the area under the curve rather than the amplitude.

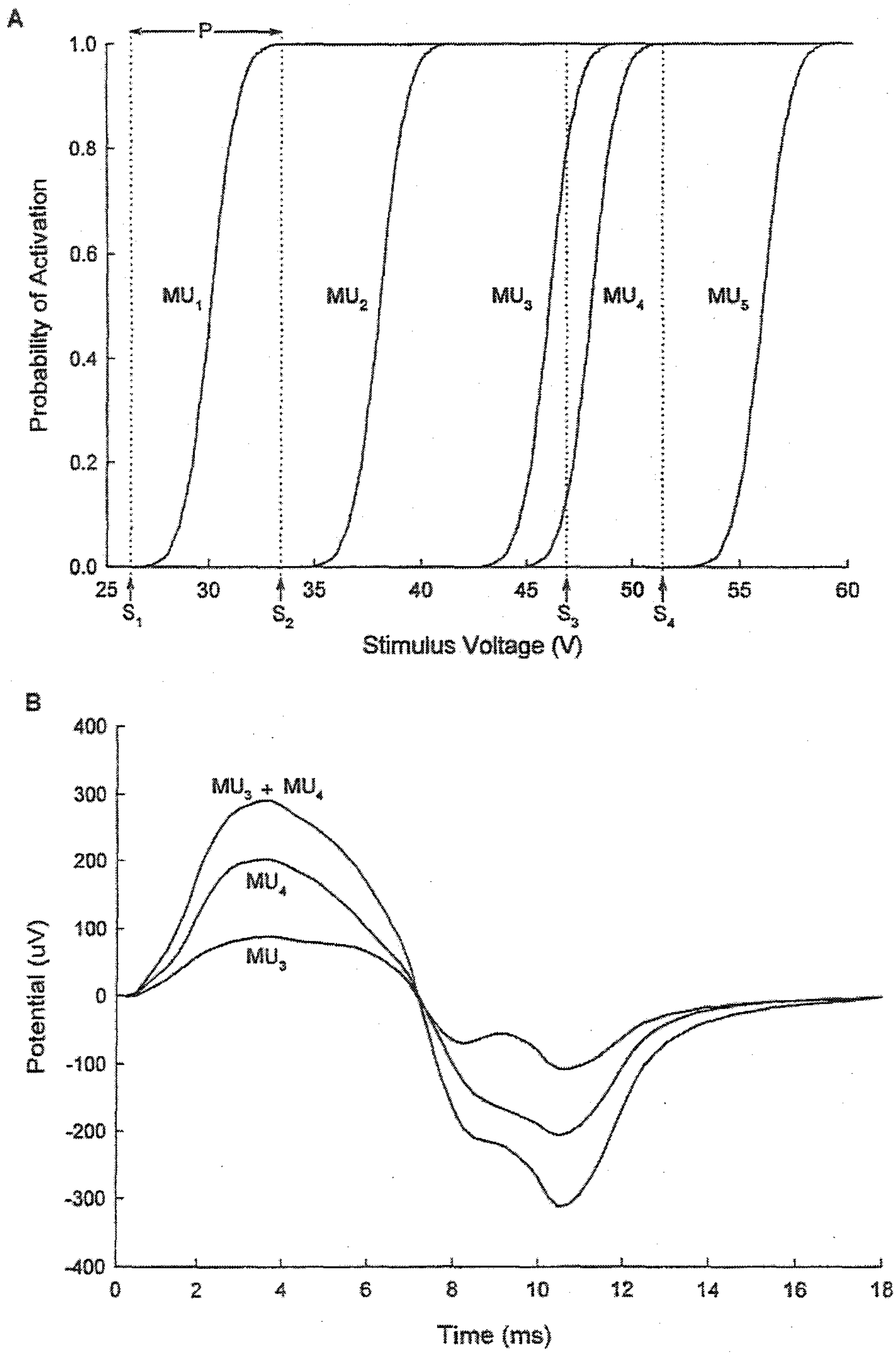

Figure 2.3. Probability of a motor unit firing (Orsi, 2000)

They reasoned this was valid because areas should sum more linearly than MUAP peak amplitudes.

In 1987, Jashenko further automated incremental MUNE by creating a computer controlled stimulator and a computer executed classification algorithm to classify M-waves. In this automated system, subjectivity was eliminated by removing the operator from determining what constitutes an increment in the CR. In the automatic system a sub-threshold stimulating pulse was applied to the nerve bundle and the response was recorded and stored in the computer as "template 1". The stimulus amplitude was automatically increased to record successive evoked muscle responses. The algorithm used to determine a new evoked response calculated the absolute area between response curves and found the Euclidean distance (see Section 4.2.5) between time samples of the responses. This system considerably improved response classification and reduced chances of missing increments in the CR when compared to manual methods.

Further improvements to the automated system were made by Cavasin (1989). Cavasin developed a more efficient algorithm for stimulation control as well as a more accurate pattern classification scheme for classifying M-wave responses. His algorithm made use of power spectral coefficients using the fast Fourier transform. As the stimulus incremented, the spectral coefficients of each recorded waveform were calculated and compared with the spectral coefficients of all the stored templates. The Euclidean distances of the spectral coefficients from the new waveform and the spectral coefficients from each template were then compared to a pre-determined minimum distance, known as the threshold. If the calculated Euclidean distances were larger than the threshold it was assumed a new motor unit had been recruited and the evoked response was stored as a new template in the EMG computer. The use of the power spectral coefficients enabled both time domain and phase information to be discarded. This eliminated problems associated with latency shifting which will be discussed later.

In Cavasin's automated system the stimulus amplitude was varied slightly around the value required for each new increment in the CR in an attempt to repeat the waveform. It was only when the waveform was repeated a minimum of three times, that it was stored as a valid new template. Once sufficient templates had been saved the individual MUAPs were extracted by a computer algorithm that ranked the stored templates in order of absolute area. Each template was subtracted from the next largest, thus producing a family of MUAPs. The Cavasin technique examined the method of using the average MUAP feature rather than the average MUAP contribution and found that this resulted in underestimation of the MUNE. He concluded that the average contribution as described earlier in this thesis is the best method. It was estimated that 200 to 400 stimuli were applied to the subject throughout the test which usually lasted 2 to 3 minutes.

2.8 Summary

In this chapter some of the anatomical and physiological aspects of MUAP generation have been discussed. MUNE, specifically the McComas technique, has been introduced, including assumptions and limitations. MUNE is still an ongoing area of research and development and several different techniques have been proposed (e.g.

Daube, 2003). In all these techniques, M-wave features have been recognized and compared either visually or automatically. The remaining chapters of this thesis address the issue of feature selection in M-wave classification in order to make the McComas technique more reliable.

CHAPTER 3
SIGNAL PROCESSING BACKGROUND

3.1 Introduction

As described in Section 2.6, MUNE has historically progressed from manual construction of the CR, to automated classification performed by a computer. The recorded M-waves used in the creation of the CR are often contaminated by physiological or environmental noise. An experienced operator is capable of recognizing these noise sources and thus, classifying M-waves into appropriate clusters to form the CR. However, an automated system using signal processing tools such as Fourier and wavelet analysis can greatly improve the efficiency of M-wave pattern recognition and removes operator subjectivity in the selection of M-waves.

Classification of recorded M-waves into a CR, whether performed manually or automatically, follows a typical pattern recognition scheme.

1) Feature Extraction: First the features of the signal that are known to contain information that separates one group of M-waves from another must be defined.
2) Discriminator Value: Next, the features must be mapped into a numerical vector that is in a particular range for different M-wave clusters. A discriminatory threshold must be defined as the separator between the vectors of different clusters.

3) Classification: Finally, a newly recorded M-wave may be classed into one of the pre-defined clusters or into a new cluster, by comparing the mapped numerical vector with the discriminatory threshold.

This thesis investigates all three steps in the pattern recognition scheme. Feature selection is of primary importance in pattern classification as it is directly linked to the speed and the accuracy with which the classification may be performed. In other words the feature set should be minimally dependent on additive noise and maximally sensitive to the M-wave characteristics.

Often in the past, M-wave pattern classification schemes have made use of time domain features to form the CR. However, frequency domain analysis with the Fourier transform and time-scale analysis with wavelets enable a clearer distinction between M-wave clusters. This thesis investigates M-wave pattern classification using of both power spectral features as obtained through Fourier analysis and wavelet vectors as obtained from a dyadic approach to signal decomposition. This chapter gives the necessary mathematical background to understand both power spectral and wavelet based analysis.

3.2 Power Spectral Features

The power spectrum of a signal is obtained by taking the square of the magnitude of the Fourier coefficients. Fourier analysis separates a signal into sinusoids of different frequencies. This is a tool for mathematically transforming a signal from a time-domain representation to a frequency-domain representation. The frequency spectrum of a signal can be viewed as a unique characteristic that may serve to match or distinguish one signal from another.

The Fourier transform is mathematically defined through the following equation:

$$F(\omega) = \int_{-\infty}^{\infty} f(t)e^{-j\omega t}\,dt$$

The signal, f(t) is multiplied by a complex exponential and summed over all time to give a series of Fourier coefficients F(ω). Each Fourier coefficient has a certain magnitude and phase associated with a sinusoid of particular frequency ω that is a component of the original signal. The larger the magnitude of a Fourier coefficient at a particular ω, the more significant contribution a sinusoid of that frequency makes to the signal.

The transform defined above requires integration. Thus, the signal f(t) must be describable by elementary functions such as sinusoidal functions, exponential functions or terms from a power series. In most practical situations, this is not the case and the Fourier coefficients must be computed through a numerical algorithm. For discrete time, or sampled signals, such as those presented in this thesis, the discrete-time Fourier transform (DFT) may be used to calculate the frequency spectrum. This transform operates on the sampled signal to produce an approximate frequency spectrum of the original analog signal. The frequency (ω) axis is then discretized. For a bandlimited signal with sampling frequency Ω, the ω axis is discretized as follows:

$$\omega_n = \frac{2\pi\Omega n}{N}, \qquad n = \frac{-N}{2},\ldots,\frac{N}{2}$$

where N is the number of data samples. The integral in the Fourier transform defined above is now approximated as a sum:

$$F(\omega_n) = \frac{1}{\Omega}\sum_{k=0}^{N-1} f\left(\frac{k}{\Omega}\right) e^{\frac{-j\omega_n k}{\Omega}}$$

A more efficient algorithm for computing the DFT is known as the fast Fourier transform (FFT). This algorithm works on the premise that N is continuously divisible by 2. A DFT of length N is written as the sum of two DFTs of length N/2. This is done recursively until the DFT of only two data points is remaining. If N is not an integer power of 2 it can be made so by padding the signal with zeroes. When padding is applied, the signal is generally multiplied by a smoothing window such as the Hamming window to ensure a smooth transition from the actual data points in the signal to the additional padded zeroes.

In MATLAB the FFT is computed using the Cooley-Tukey (1965) algorithm. This algorithm assumes that the signal length N can be written in composite form as $N=N_1N_2$. The algorithm then computes N_1 transforms of size N_2 and N_2 transforms of size N_1. This process is performed recursively for both the N_1 and N_2 DFTs until a point is reached where the problem can be solved using machine generated "codelets". The execution time for this algorithm depends on the length of the signal and is fastest when the number of data points, N is a power of 2.

Though the Fourier transform is applied in many practical signal processing applications, there is an important characteristic of the transform that needs to be recognized. This is that the Fourier transform is reversible. The transform allows time information to be converted to frequency information and vice versa. However, only one set of information is available at any given instance. For example, when the frequency information of a signal is known through the Fourier transform, no information about the signal in time is known. This potential drawback is of no consequence if the signal in question is stationary or if frequency information alone is sufficient. Yet if the signal is contains important transient characteristics or is non-stationary, Fourier analysis is not suitable. The M-waves examined in this thesis, are both transient and non-stationary. For this reason, alternate feature extraction techniques, primarily wavelet analysis are examined.

3.3 Short-Time Fourier Transform

The Short-Time Fourier Transform (STFT) introduced by Gabor (1946) is a modification of the Fourier transform in an attempt to retain both time and frequency information for a signal under analysis. The STFT produces a two dimensional function with time and frequency as variables. Thus, the STFT gives information about when in time a given frequency component occurs. However, the precision of this information is limited and in effect a compromise between time and frequency information exists.

The STFT premise is that, while a signal may not be stationary, small segments of the signal can be assumed stationary. These segments are captured by a window with a width equal to the segment of the signal where stationarity is valid. The signal and the window are multiplied to extract the stationary segment. The Fourier transform of the segment is then computed.

In the STFT, the window length is of utmost importance. Longer window lengths provide greater frequency resolution while narrow lengths provide greater time information. The downfall is that once a window length is chosen for a particular signal it is fixed for all frequencies. Most practical signals contain high frequency components for a short duration and low frequency components for long duration. Representing such a signal using the STFT, when a narrow window is chosen there is adequate time resolution at the higher frequencies but limited the frequency resolution in the lower ranges. Conversely, if a wider window is chosen, the higher frequency components will not be resolved. A more desirable approach is one in which the window size can be varied. This is captured in wavelet analysis.

3.4 Wavelet Analysis

In wavelet analysis, the spectral components are not resolved equally as in the STFT. Instead, wavelets are designed to yield enhanced time resolution and reduced frequency resolution at high frequencies and enhanced frequency resolution and reduced time resolution at lower frequencies. This is the optimal approach for signals that have low frequency components for long durations and high frequency components for short durations.

The term wavelet describes a waveform of limited duration that has an average value of zero. Wavelets are generally asymmetric and irregular as opposed to the continuous smooth sinusoids used in Fourier analysis. Figure 3.1 shows a typical wavelet derived from a family of mother wavelets known as the Daubechies family.

In Fourier analysis, the signal under investigation is decomposed into a series of sine waves at different frequencies. In wavelet analysis the signal is decomposed into a series of scaled and shifted versions of a mother wavelet. The wavelet transform is defined mathematically as:

$$C(scale, position) = \int_{-\infty}^{\infty} f(t)\Psi(scale, position, t)dt$$

The transform results in a series of wavelet coefficients that are dependent on the scale and position of the mother wavelet. The coefficients, when multiplied by a wavelet of the correct scale and position yield the wavelets composing the original signal. The wavelet transform effectively acts as a correlator between the shifted, scaled mother wavelet and segments of the signal. For shifted and scaled values where the correlation with the signal segment is high, the coefficient will be large whereas for shifted and scaled values where the signal segment and the wavelet remain uncorrelated the coefficient will be low. The scaling factor corresponds to stretching or compressing the mother wavelet and is thus responsible for deriving the frequency characteristics of the signal. When the scaling factor is large, the mother wavelet is stretched and is compared to a longer segment of the signal. In this case, the coefficients represent the lower frequency components of the signal. For low scaling values, the more compressed the mother wavelet and the smaller the segment of the signal that is compared. In this case, the coefficients represent the higher frequency components of the signal. The shifting factor merely delays the onset of the wavelet enabling different segments of the signal to be compared to the wavelet.

The continuous wavelet transform calculates the wavelet coefficients at every possible scale and position and is not a practical approach to wavelet decomposition. A more efficient analysis is achieved by computing the coefficients at a subset of scales and positions that are based around powers of 2. These are known as dyadic scales and positions and when used, yield the discrete wavelet transform (DWT) as given by:

$$C(a,b)=\frac{1}{\sqrt{a}}\int_{-\infty}^{\infty}f(t)\Psi\left(\frac{t-b}{a}\right)dt$$

where,

$$a=\frac{1}{2^{j}},b=\frac{k}{2^{j}},(j,k)\in Z$$

This dyadic DWT can be efficiently implemented using the Mallat algorithm (Mallat, 1989). This algorithm builds on a two-channel sub-band coder using quadrature mirror filters. This implementation is shown schematically in Figure 3.2. The coefficients representing the low frequency components of the signal are known as the approximation coefficients while those representing the higher frequency components are termed the detail coefficients. Figure 3.1 (A) shows the filter coefficients used for Mallat decomposition with a Daubechies 5 mother wavelet.

In the implementation shown in Figure 3.2 the signal, S, is passed through high and low pass filters to produce two new signals. Each of the new signals contains as many data points as the original and so is down-sampled to correct for doubling in the data. In Figure 3.2, the length of the resulting approximation (cA) and detail (cD) signals is greater than half the length of the original signal due to the extra samples included as a direct result of the filter convolution.

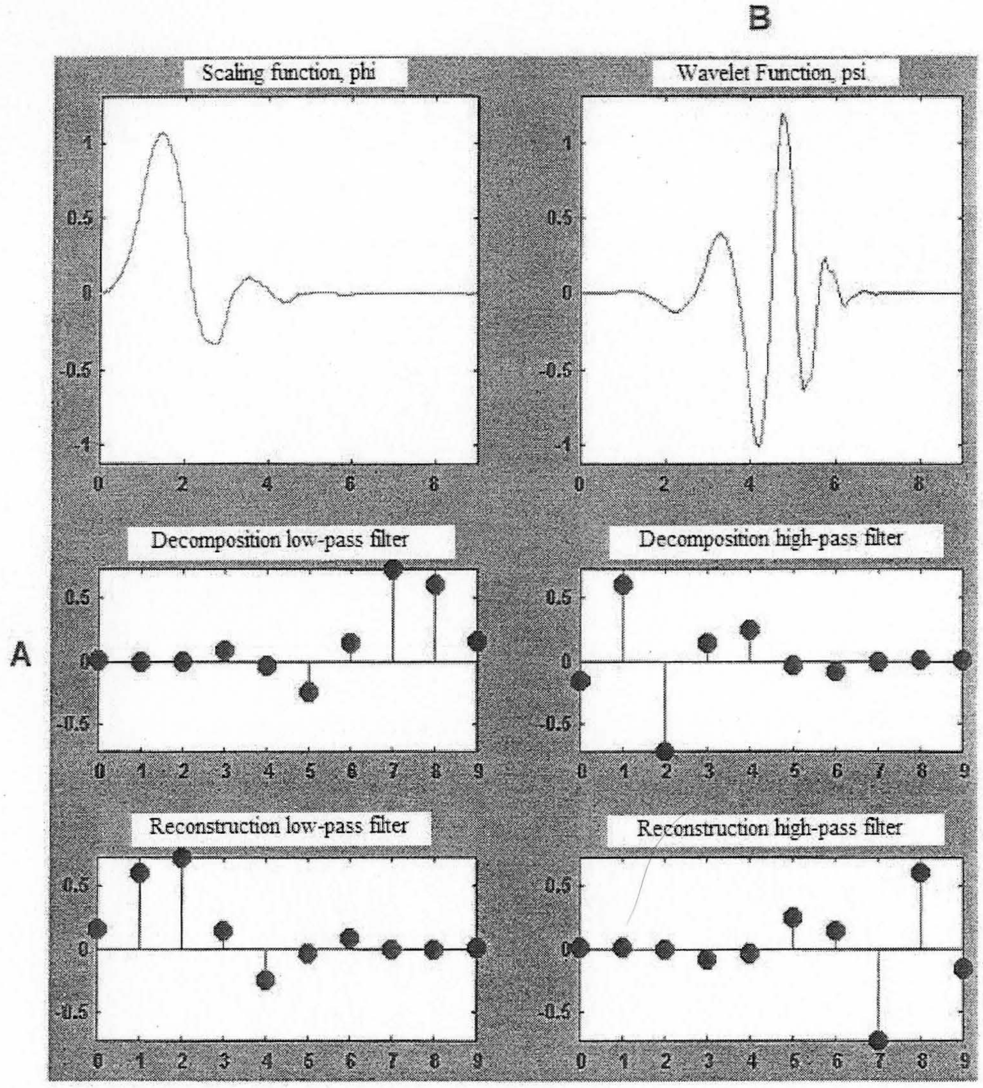

Figure 3.1. Daubechies 'db5' (A) filter representation and (B) wavelet function (Orsi, 2000)

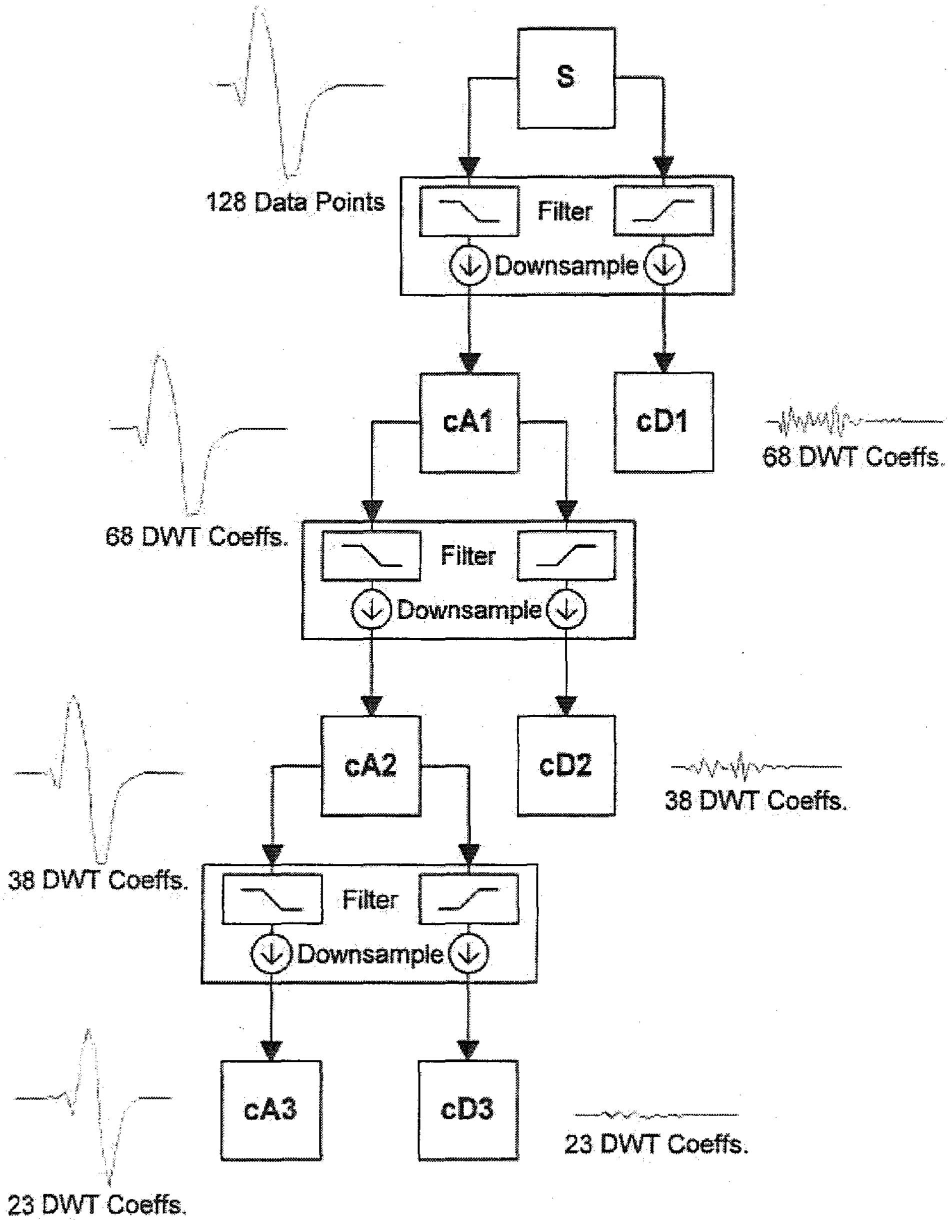

Figure 3.2. Dyadic wavelet decomposition (Orsi, 2000)

The decomposition process is iterative with each successive level, decomposing the low frequency components of the signal into smaller frequency bands. The decomposition can continue until the details band consists of a single sample. In practice a suitable number of decomposition levels can be determined by examining the nature of the signal using either an entropy measure or by examining the power spectral density as described in Section 5.5.

3.5 Time-Invariant Wavelet Analysis

As discussed above, the wavelet transform has distinct advantages over the Fourier transform for the analysis of transient signals. However, the wavelet transform is still far from ideal. One inherent difficulty presenting problems for M-wave pattern recognition is the wavelet transform's sensitivity to translations. In practice, the wavelet coefficients of two signals may differ greatly even when the two signals are merely time shifted versions of each other. This complicates pattern recognition when the signals are to be clustered based on shape and amplitude and not on time delays. Several algorithms exist to correct this problem by creating a wavelet that is time-invariant.

It is intuitive that a modification introducing circular shifts to the Mallat algorithm will eliminate the sensitivity to translations felt by the wavelet transform. Specifically, if for each level of decomposition the input to the filter bank is circularly shifted by 1, the output will be a set of vectors, differing because of the shifted input. Identical but time-shifted signals will result in identical sets of vectors at each level as they will both be circularly shifted at the input. If all of these output vectors are retained, identical translated signals will have matching wavelet coefficients. However, this process is not efficient as many of the computations produce results that are redundant. The algorithm used for a shift-invariant wavelet in this thesis eliminates this redundancy while still retaining the shift-invariant property. This algorithm is known as the multi-scale wavelet representation or MSWAR (Sari-Sarraf and Brzakovic, 1990). Essentially the algorithm serves to modify the Mallat implementation as shown in Figure 3.3.

In MSWAR, in the first level of decomposition the signal is passed through the wavelet high and low pass filters. In addition, the original signal undergoes a circular shift by 1 and this shifted version is passed through the same filters. The resulting two outputs from the high pass filter are down-sampled. Down-sampling is subsequently followed by each of the signals being stretched to double their length. Lastly, one of the two high pass filter outputs is shifted by 1 and added to the other. The result is a signal approximating a 1st level detail coefficient and containing information from both the original signal decomposition and the decomposition of a circularly shifted version of the original signal. The approximation vectors on the other hand, are not stretched, shifted and added, but are instead passed to the next iteration where the circular shift occurs again. The process is repeated for all levels of decomposition. Though this algorithm is computationally more involved than the traditional wavelet transform it is invaluable for the pattern recognition of translated signals.

In the following chapters, the mathematical transforms described above are used to extract M-wave features for pattern recognition. The relative success of the classifiers is determined and insight is given into the best performing feature extractor.

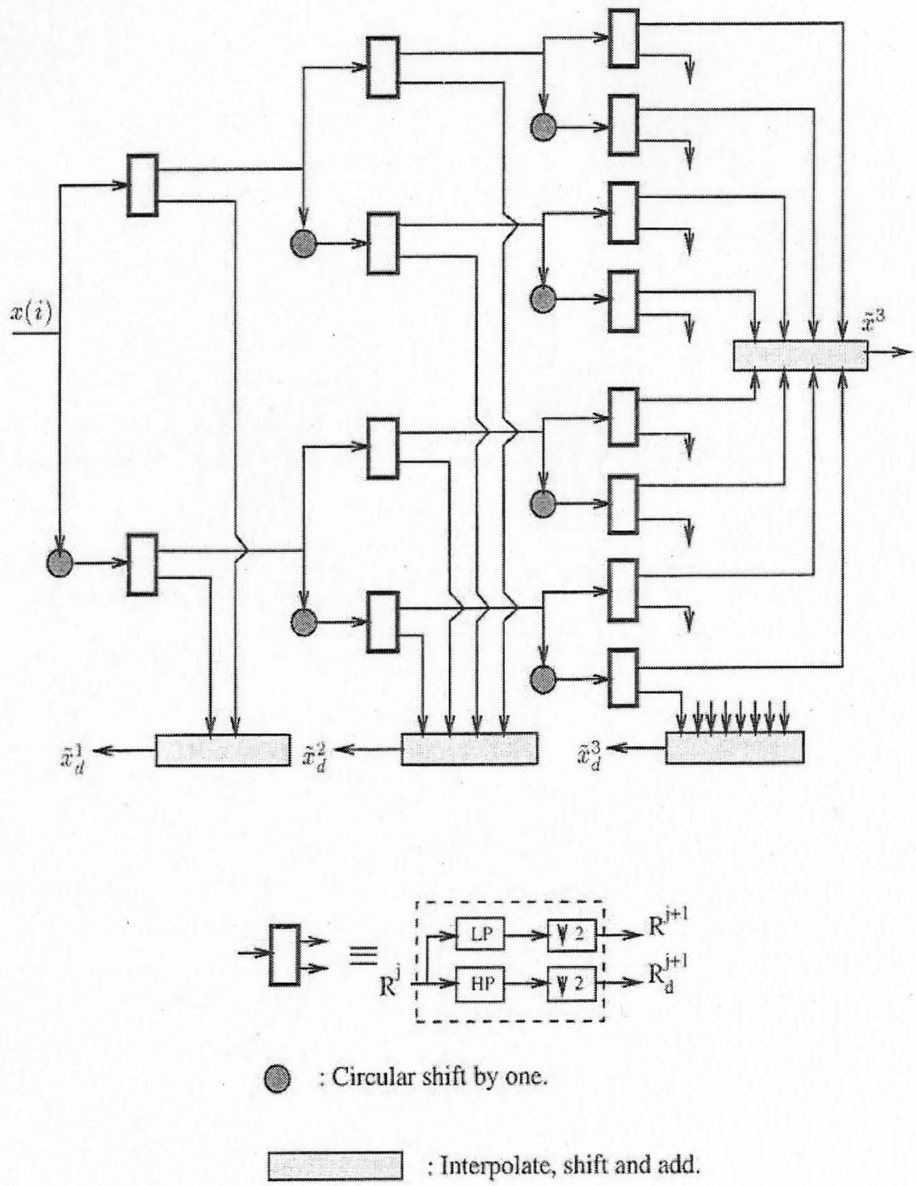

Figure 3.3. Implementation of a shift-invariant wavelet (Sari-Sarraf and Brzakovic, 1990)

CHAPTER 4
MEASUREMENT AND ANALYSIS SYSTEM

4.1 Introduction

To evaluate the benefits of the wavelet transform in M-wave pattern recognition a system capable of measuring and analyzing single channel EMG recordings was designed. The initial processing algorithms were developed offline using MATLAB 7.0 and pre-recorded M-wave files. This allowed for preliminary testing to develop optimal noise reduction and classification schemes used later to create a real-time LabVIEW system for signal collection and pattern recognition. The system enables the user to select between Fourier or wavelet pattern recognition techniques for real-time classification of M-waves recorded from a subject. In addition, all M-waves are stored for later off-line analysis. Furthermore the system is equipped with an adjustable threshold setting to evaluate the effects of different discriminators to enable muscles other than the thenar to be tested. The main hardware components are electrodes, an amplifier and a stimulator, a National Instruments NI 6024E (Austin, Texas, United States) data acquisition board with A/D and D/A capabilities and a personal computer with LabVIEW software. An overview of the hardware set-up is shown in Figure 4.2. The software is discussed in further detail in Section 4.2.

4.1.1 Subject Set-up

The subjects were seated comfortably with the hand resting on a table and forearm comfortably supported on the table. The hand was further supported with sand bags to minimize subject movement and increase comfort level. The comfort of the patient was found to be important as patients that were not relaxed demonstrated a higher level of voluntary MU activity that interfered with the desired evoked M-wave recording.

4.1.2 Electrodes

The recording electrodes were made from disposable self adhesive ECG electrodes (Product No: 30807732, Tyco Healthcare Group, Mansfield, MA). The recording electrode was constructed by cutting the 25mm by 23mm electrode longitudinally. The halves were placed end to end over the thenar eminence to cross the first metacarpal bone perpendicularly at the junction of its proximal and middle thirds as shown in Figure 4.1. An additional half of an ECG electrode, used for reference, was attached to the proximal phalanx of the thumb. A ground electrode was located at the dorsum of the hand. All connections were made using lightweight alligator clips for flexibility. Moreover, the stigmatic and reference electrodes were connected to the amplifier via a shielded cable to reduce the effect of external noise.

4.1.3 EMG Amplifier

All recorded signals were amplified and band-passed filtered using an A-M Systems 1700 differential amplifier (A-M Systems, Sequim, WA) with high-pass and low-pass settings at 10 Hz and 500 Hz respectively. The gain of the amplifier was typically set at 1000 for subject collections.

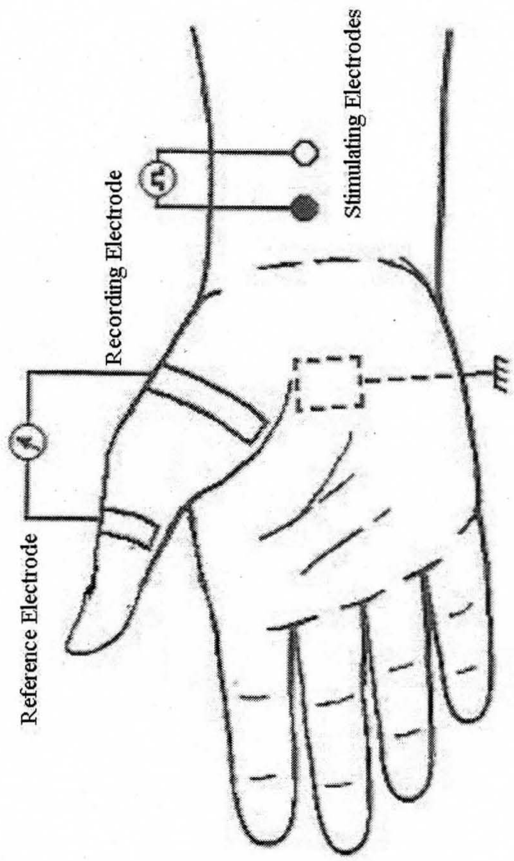

Figure 4.1. Experimental Instrumentation

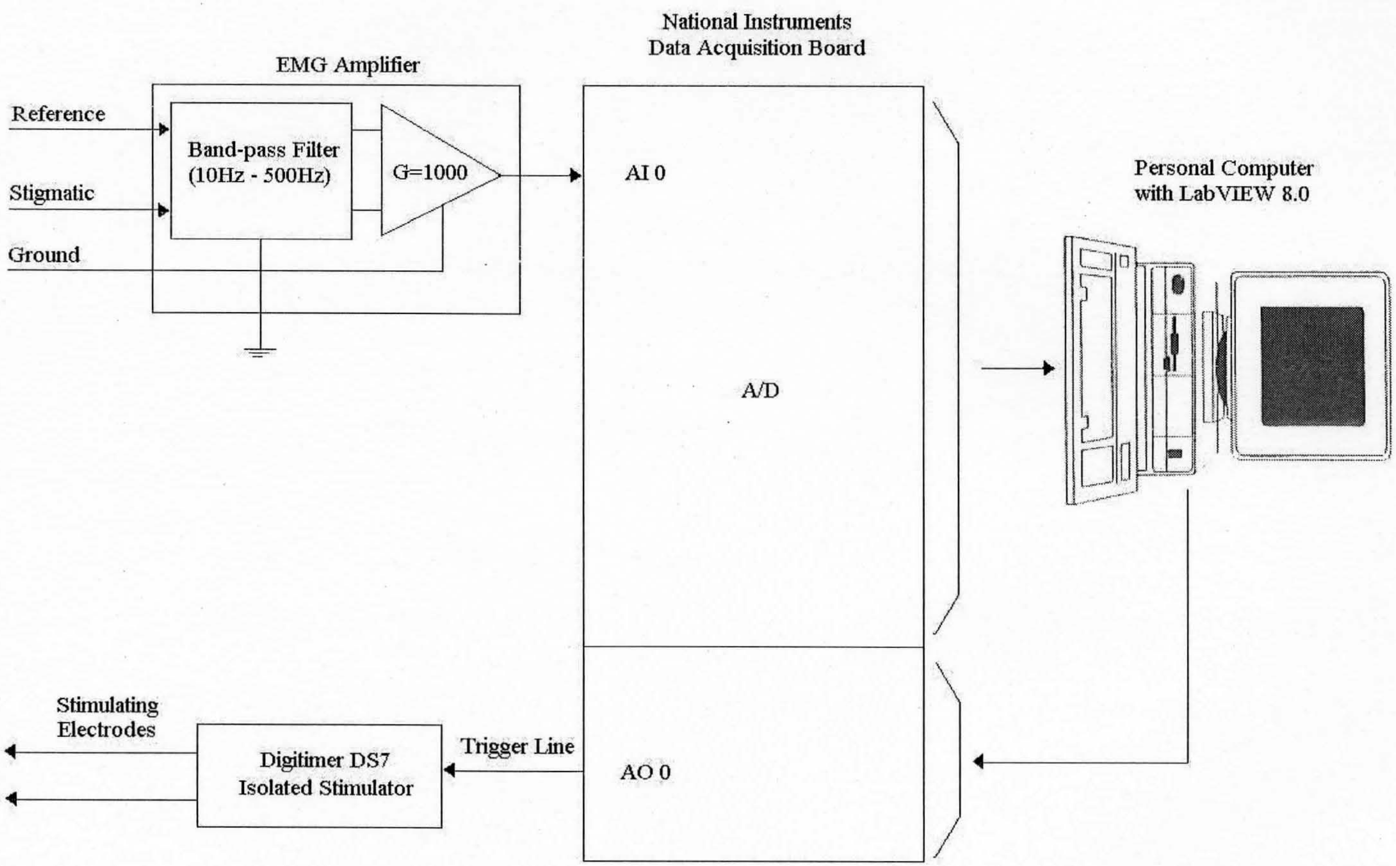

Figure 4.2. Hardware Overview

4.1.4 Stimulator

The stimulator used for this system was a Digitimer DS7 (AM Systems, Sequim, WA) constant current isolated stimulator. A trigger pulse was invoked by the software through one of the digital outputs on the data acquisition board at a rate of 1 Hz. The stimulating pulse width was set to 100 microseconds to minimize patient discomfort. The stimuli were delivered through 6 mm diameter stainless steel electrodes mounted 1.8 cm apart on a plastic bar. The plastic bar was strapped over the median nerve proximal to the wrist. The bar position was moved slightly on initial set-up to find the optimal placement. This was the position where there was little lumbrical or forearm muscle co-stimulation. The stimulus amplitude level was manually controlled during this experiment. With the help of the software displays the operator was efficient in determining which levels of stimulation needed to be further explored to obtain all levels of the composite response while keeping alternation at a minimum.

4.2 Software

The software for this thesis was created using LabVIEW 8.0 Full Development System (National Instruments, Austin, Texas, United States). LabVIEW was chosen for this project as it is especially created by National Instruments to interface with their development boards. Additionally, LabVIEW is an intuitive graphically oriented programming language equipped with a built-in library of pre-programmed functions called visual interfaces (VIs). The VIs are capable of handling I/O, signal processing, statistics, mathematics, file manipulation and graphing functions while at the same time allowing the programmer access to the code thus increasing LabVIEW's versatility. The graphical user interface displayed during a typical recording session is shown in Figure 4.3

The MUNE implemented in the software in this system is based on the McComas incremental technique which was automated first by Jasechko (1987) and later improved by Cavasin (1989). Some of the concepts in this thesis are modified versions of those used in these automated systems (e.g. baseline correction). Figure 4.4 shows the software flowchart while Figure 4.5 describes the M-wave pattern classification method in detail.

4.2.1 System Parameters

The parameters needed for the software program to execute are selectable by the user. These parameters cannot be changed during a recording session and thus must be set appropriately before a recording session is started. The default values were determined empirically for the thenar muscle and are automatically loaded when the program is called. However, these values can be altered before the START button is pressed. This feature enables the software to be easily adapted for studying alternate muscles.

A

B

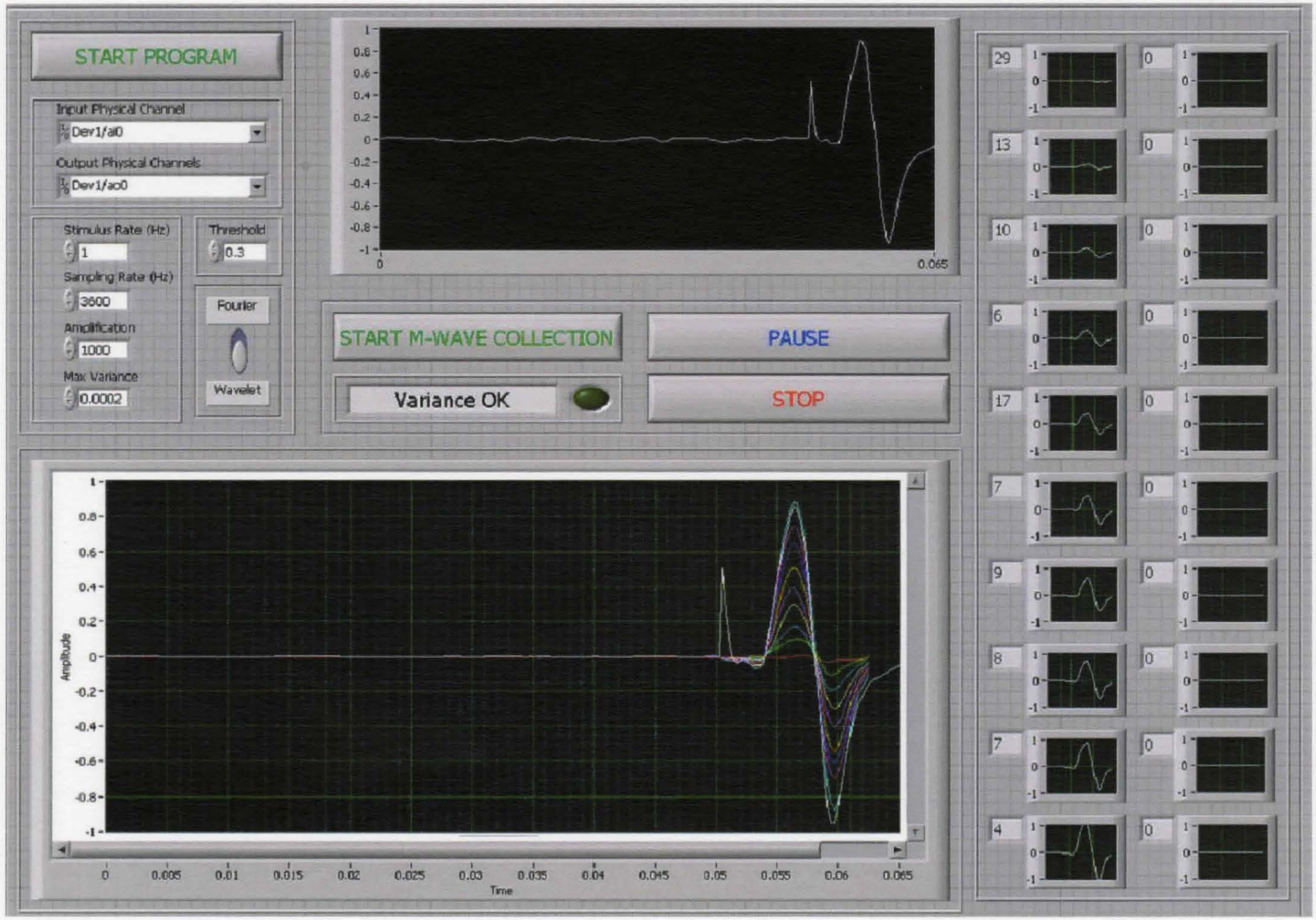

C

Figure 4.3. LabVIEW Program Front Panel. A: Controls, parameters and raw data display. B: Noise reduced raw data and previously defined templates. C: Individual template display windows.

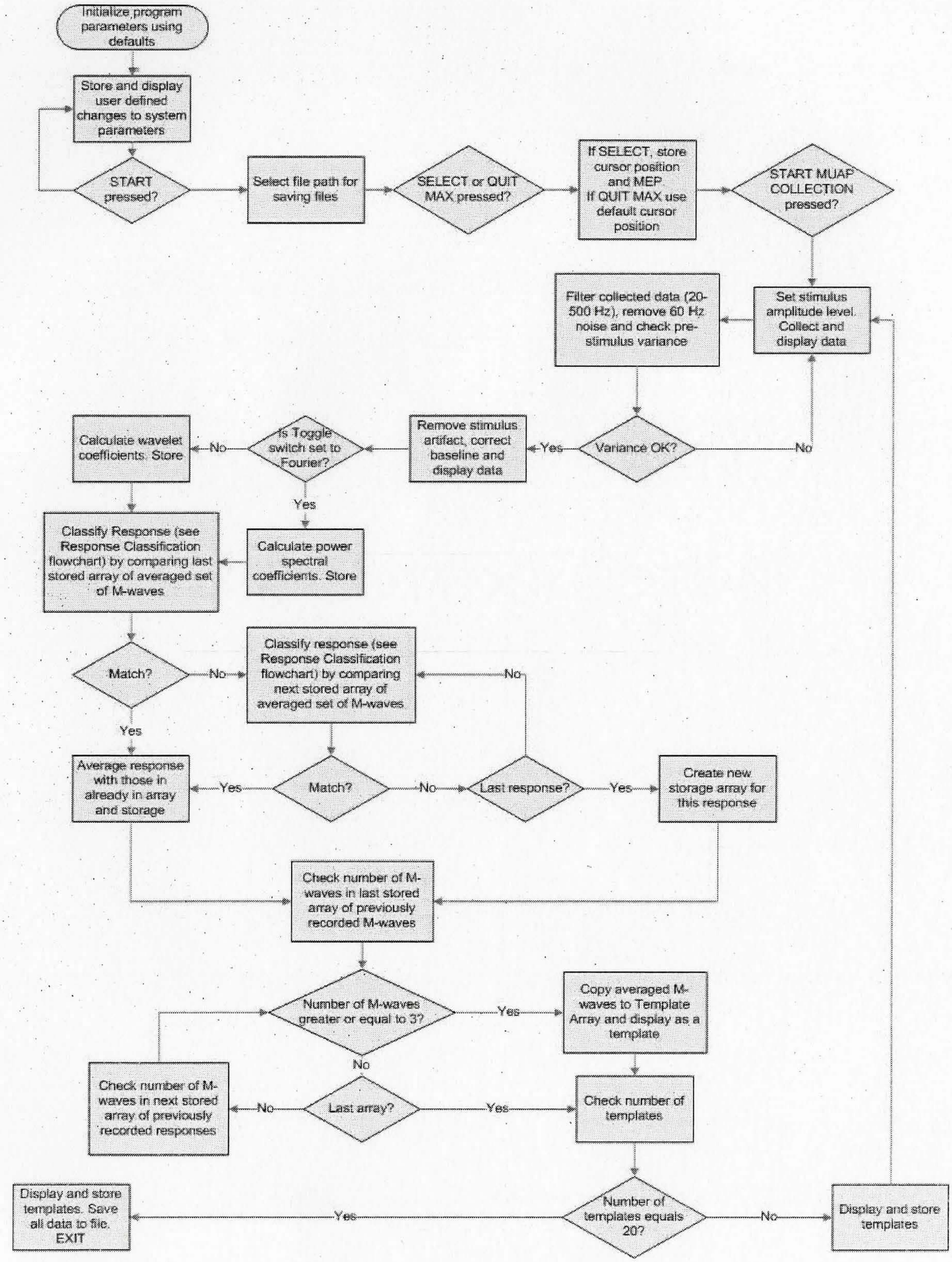

Figure 4.4. Software Flowchart

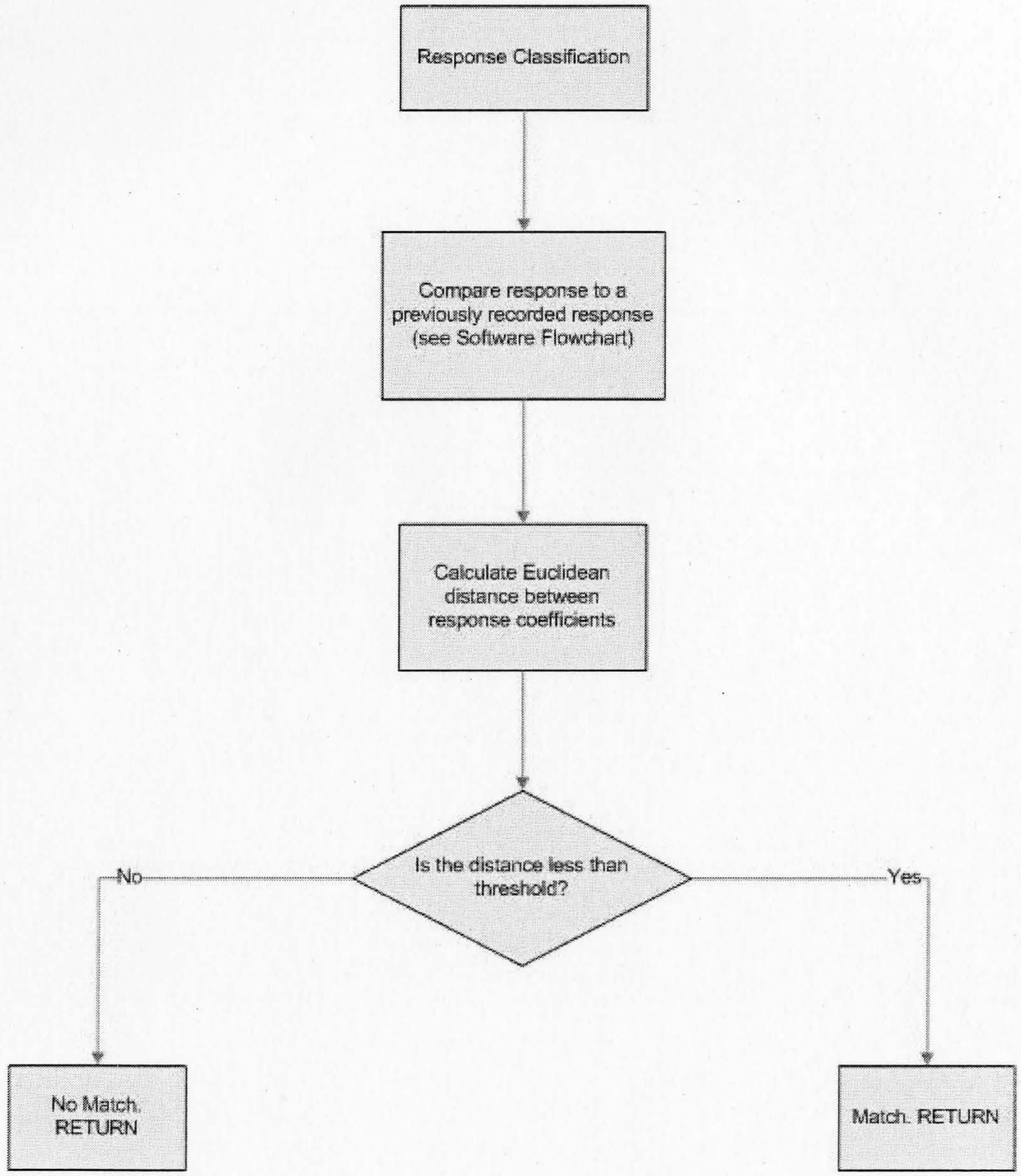

Figure 4.5. Response Classification Flowchart

4.2.2 Synch AIAO

A sub VI named Synch AIAO was created to trigger the stimulator and collect data. Parameters from the main program are passed to Synch AIAO. These include sampling rate (default 3600 Hz), amplification (default 1000), pre-stimulus length (50 ms) and post-stimulus length. The Synch AIAO sub VI is then initiated and collection begins. Two segments of EMG data are collected by the Synch AIAO routine. The first is collected before the application of the stimulus and is known as the pre-stimulus data. The pre-stimulus window is a fixed length of 50 ms and the data is used to determine external sources of noise and background EMG. The second segment of collected data occurs immediately after the stimulus. This is the post-stimulus data and contains the stimulus artifact and the evoked muscle response as shown in Figure 4.6 (A). The post-stimulus window may be of varying length and is dependent on how the user configures the Maximum Evoked Potential collection routine as explained later.

The Synch AIAO routine is designed to send a triggering waveform to the stimulator along Analog Output 0 (AO0) while simultaneously collecting data along Analog Input 0 (AI0) on the National Instruments data acquisition board. The timing is such that the collection will occur only for the duration of the triggering waveform. Thus, the length of the triggering waveform is important and the waveform must be created after the user-defined parameters such as post-stimulus length and sampling frequency are determined. In Figure 4.6 (B), the triggering waveform corresponding to the collected data is shown. As seen the figure the trigger pulse is delayed within the waveform. This enables the pre-stimulus data segment to be collected. The trigger pulse itself remains

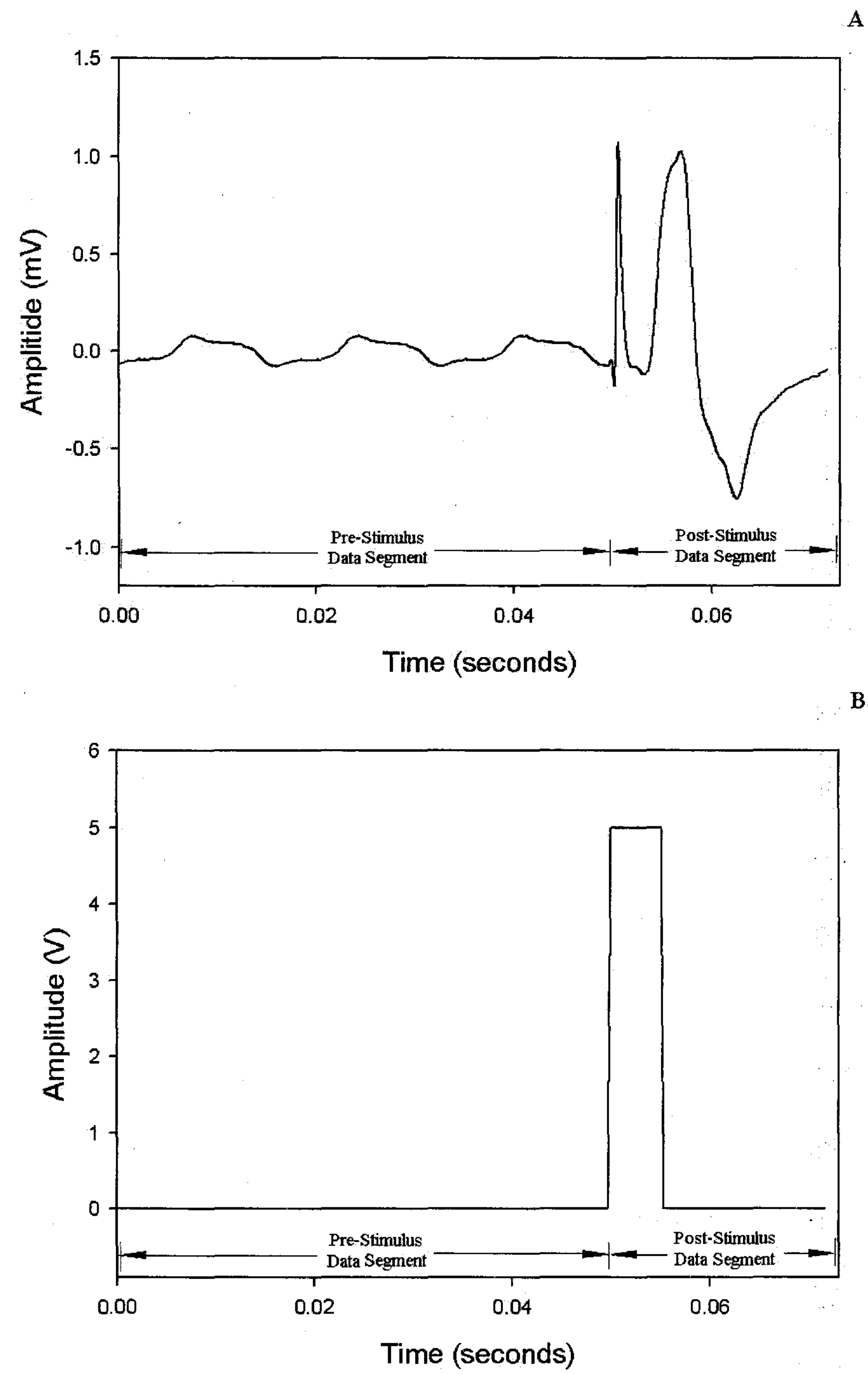

Figure 4.6. Typical raw data recording from human thenar muscle (A) and triggering waveform (B)

high for 5 ms. Though the stimulating box is positive edge triggered it was found that the pulse must remain high for a sufficient period of time for proper operation.

Once the post-stimulus data is collected a timer prevents the next data collection from occurring for a specified duration. The duration is specified by the user defined parameter Stimulus Rate, whose default value is 1 Hz. During this waiting period the trigger line is held at 0 and no data is recorded or displayed. Also during this time the data that was just recorded passes through signal processing, feature extraction and classification routines.

The Synch AIAO routine serves only to trigger the stimulator and not to control the amplitude of the stimulating pulse. Automated stimulator amplitude controls were implemented by Jasechko (1987) and Cavasin (1989). However, in this experiment, greater flexibility was needed and it was therefore decided that the stimulator be under manual control by an experienced operator.

4.2.3 Signal Processing

The processing algorithms described here were developed off-line using MATLAB 7.0. They were then implemented in LabVIEW 8.0 and applied to all on-line data collections that passed a pre-stimulus variance check defined in detail below. The original MATLAB 7.0 algorithms were retained and augmented to simulate the real-time LabVIEW system. These algorithms are useful for off-line experimentation with pre-recorded data.

4.2.3.1 Differential 60 Hz Noise Reduction

A common problem in biological signal recordings is 60 Hz noise caused by a capacitive coupling of power sources to a subject's skin and recording leads. In EMG, this source of noise is particularly troublesome because the M-Wave responses contain information in the 60 Hz frequency range. For this reason most filtering techniques, while removing the 60 Hz noise, cause a distortion of the desired M-wave signal.

For this system, it was determined that 60 Hz noise could be most successfully reduced by coherent detection and elimination. Figure 4.7 (A) shows a typical recording before processing. In most physiological recordings, the 60Hz noise presents as a 60 Hz sine wave and this can be removed by simply adding a 60Hz signal with the same amplitude and phase shifted 180°. In the earlier recordings, this was the case. However, since then, the hospital (McMaster University Medical Center) implemented its own generating plant, attached to the power grid, and the capacitively coupled noise, shown in Figure 4.7 (A). now has a more complex form. The signal has a fundamental 60 Hz frequency and is highly periodic. This required a modified coherent detector.

Figure 4.7 (B) shows the signal after the coherent detection and elimination algorithm is applied. This algorithm first extracts the pre-stimulus data and uses this to detect the presence of periodic noise and to determine its amplitude and phase. The pre-stimulus data is smoothed by passing it through a band pass filter with pass band range 20-100 Hz. Next, the locations of the peaks and troughs are found. The presence of 60 Hz noise is determined by an algorithm that determines the time between the first and second peaks and the first and second troughs in the pre-stimulus data. If this time

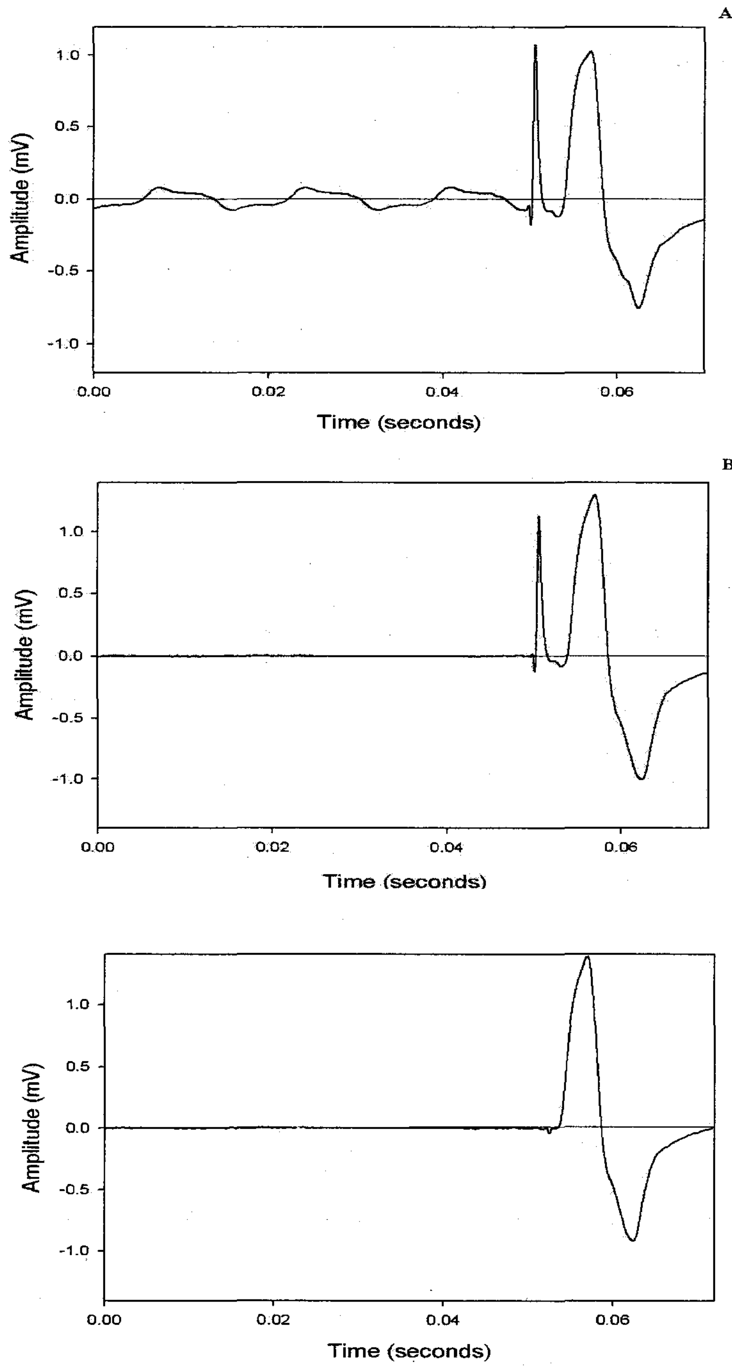

Figure 4.7. Signal Processing. (A) Raw data signal. (B) After 60 Hz noise reduction. (C) After elimination of stimulus artefact and correction of baseline.

difference is within 6% of the period for 60 Hz, it is presumed that this type of noise is present.

Once the presence of periodic noise with 60 Hz fundamental frequency is verified, a template that has the same amplitude, phase and shape as that contaminating the signal is created. This template can then be subtracted from the entire recording to coherently remove the 60 Hz noise. The template is created by capturing one 16.6 ms period of noise from the pre-stimulus data. The captured period is then repeated to form a template of sufficient length. The phase difference between the noise in the pre-stimulus data and the created template is found and the created waveform is shifted to align with the recorded noise. To finally remove the 60 Hz, the created waveform is subtracted from the entire recorded signal.

This method was chosen because synch pulses on the power lines in the recording environment cause the 60 Hz noise in the data collection to have a distinctive shape that is not perfectly sinusoidal. Although based on 60 Hz periodicity, this noise reduction approach can be used to remove any periodic noise from physiological recordings.

4.2.3.2 Stimulus Artifact Removal

The post-stimulus data segment which contains the desired M-wave response and the stimulus artefact must be further processed before pattern classification can be performed. This further processing consists of removing the stimulus artifact. In addition, the descending baseline that is attributed to the stimulus artifact and that underlies the M-wave response must be adjusted. Both the stimulus artifact and the descending baseline are evident in figure 4.7 (B).

The stimulus artefact is easily removed by re-segmenting the post-stimulus window and ignoring the remaining data. In a sub VI called Eliminate Stimulus Artifact, the post-stimulus window is shortened by ignoring the first 3 ms. The first 3 ms of the post-stimulus window is where the stimulus artifact occurs. Thus, ignoring the data during this time effectively removes the stimulus artifact.

Correcting for the descending baseline is slightly more complex. It is necessary that this descending baseline be removed since the automated pattern recognition technique makes use of Fourier or wavelets to classify M-waves. The descending baseline will affect the Fourier and wavelet coefficients, whose values are essential in the pattern classification scheme. As the baseline in different collections may descend differently, it introduces additional features aside from the M-wave features that will be used to classify the responses. This will introduce errors in the results.

The descending baseline is removed by performing a linear correction. The baseline descent is approximately linear over the 20-30 ms of the M-wave duration. A line is created by interpolating between the first and last point of the data segment created by Eliminate Stimulus Artifact sub VI. This line is then subtracted from the data segment to remove the baseline. Figure 4.7 (C) shows the M-wave response after removing both the stimulus artefact and the descending baseline. It was found that this method produces little signal distortion and effectively isolates the M-wave response which can now be used in a pattern classification scheme.

4.2.3.3 Response Rejection

Occasionally during a data collection background EMG noise, other than 60 Hz or motion artifact, may contaminate the M-wave response. As it is not possible to design algorithms that effectively remove these sources of interference, these situations must be detected and the responses rejected. To detect occurrences of such interference, the pre-stimulus data, after removal of any 60 Hz noise, is subject to a variance test. This algorithm calculates the variance of the 50 ms of pre-stimulus data. If this variance is above a specified threshold the data collection is rejected and an indicator appears on the front panel display of the program on the computer screen to notify the operator. The LabVIEW program then proceeds to give another stimulus and check the variance of the next recording. Only those data collections that pass the variance test are processed and stored as M-wave responses to be used in the pattern classification scheme.

The variance threshold was determined experimentally with the aid of an experienced operator. Once determined, the threshold was fixed for all subjects in the study.

4.2.3.4 Signal Feature Extraction

The LabVIEW interface shown in Figure 4.3 is equipped with a toggle switch allowing the operator to select either the Fourier or wavelet transforms to extract the features used for automatically classifying M-waves during a real-time data collection. Feature extraction is performed on each response directly after the response has been noise reduced and the stimulus artifact and baseline drift have been eliminated.

4.2.3.5 Fourier Transforms

When the operator sets the toggle switch on the front panel display to FOURIER, the Fourier transform is applied to the processed M-wave and the power spectral coefficients are used as response classification features. After pre-processing, the isolated M-wave response is stored in an array. Due to the fact that the post-stimulus window (see Figure 4.6) is user defined, the length of the isolated M-wave response may be different in different experimental sessions. For this reason, and for the sake of designing a robust program, the number of points used in the Fourier transform is variable and calculated automatically. The automatic calculation begins with determining the length of the isolated M-wave response. The M-wave response is then resized to the next higher valid power of 2 by setting the new trailing elements to zero and leaving the first elements unchanged. The newly sized waveform is input to the LabVIEW sub VI called FFT to calculate the fast Fourier transform. Typically, the isolated M-wave response is 20 ms. At a sampling rate of 3600 Hz, the M-wave response is then 72 points. This response is zero-padded to 128 points which are fed to the LabVIEW FFT producing 128 complex Fourier coefficients. The Fourier power coefficients are then calculated.

Though the M-wave responses are band-limited, all power spectral coefficients calculated by the LabVIEW FFT were retained and used in the pattern classification scheme. The reasoning is that coefficients representing the higher frequencies would be low values and thus, not effect the pattern classification. Moreover, the use of additional coefficients does not sufficiently increase computations and the speed of the program is not compromised.

4.2.3.6 Wavelet Transforms

Alternatively, the operator may set the toggle switch on the front panel of the LabVIEW program to WAVELET. When this is the case, the wavelet transform is applied to the pre-processed and isolated M-wave response and the coefficients are used as the spectral features for M-wave pattern classification. To begin, the M-wave response is re-sized to the next highest power of 2 as explained above for the case of the Fourier transform. Typically, re-sized responses are 128 points. The online LabVIEW program makes use of the sub VI called Wavelet Transform that implements a 3-level decomposition using the Daubechies 4 mother wavelet. A study examining the effects of different wavelet families as well as different levels of decomposition is presented in Chapter 5.

4.2.4 Experimental Protocol

The experiment begins by preparing the subject as shown in Figure 4.1. The stimulating electrode placement is tested with the stimulator under manual control by an experienced operator and the aid of a graphical display provided by the LabVIEW program. The optimal stimulating electrode placement is such that the thenar is stimulated without effecting lumbrical or forearm muscles. When the proper placement is found, the electrode bar is held in position with an adjustable strap. Next the operator increases the stimulus amplitude to reach the MEP which is subsequently stored. Following MEP recording, the sub-threshold responses are acquired by gradually increasing the stimulus amplitude. All subjects gave informed consent prior to the experiment.

4.2.4.1 MEP Collection

The front panel of the LabVIEW program is shown in Figure 4.3. The user begins by pressing the START button which calls the MEP collection window shown in figure 4.8. In this routine Synch AIAO is called at a rate of 1 Hz. Thus, the patient is subjected to stimuli every second and the response is captured on the screen. The operator increases the stimulus amplitude with a manual control until the maximum response has been reached. That is, the operator increases the stimulus amplitude until the peak-to-peak value of the M-wave response no longer changes.

The peak-to-peak value is calculated using only the portion of data located between the two vertical cursors as shown in Figure 4.8. The operator must ensure the cursors surround only the M-wave response and do not capture the stimulus artifact. The cursor position also determines the length of the post-stimulus window used later in the collection of sub-maximal responses.

Once the maximum M-wave has been found and the cursors set appropriately the user may press SELECT MEP to save the MEP and cursor position. If QUIT MEP is selected the MEP is disregarded and the cursor position is ignored. In this case, the cursor position is not used later to determine the post-stimulus window length for the sub-maximal collections. Instead the default post-stimulus length is 50 ms.

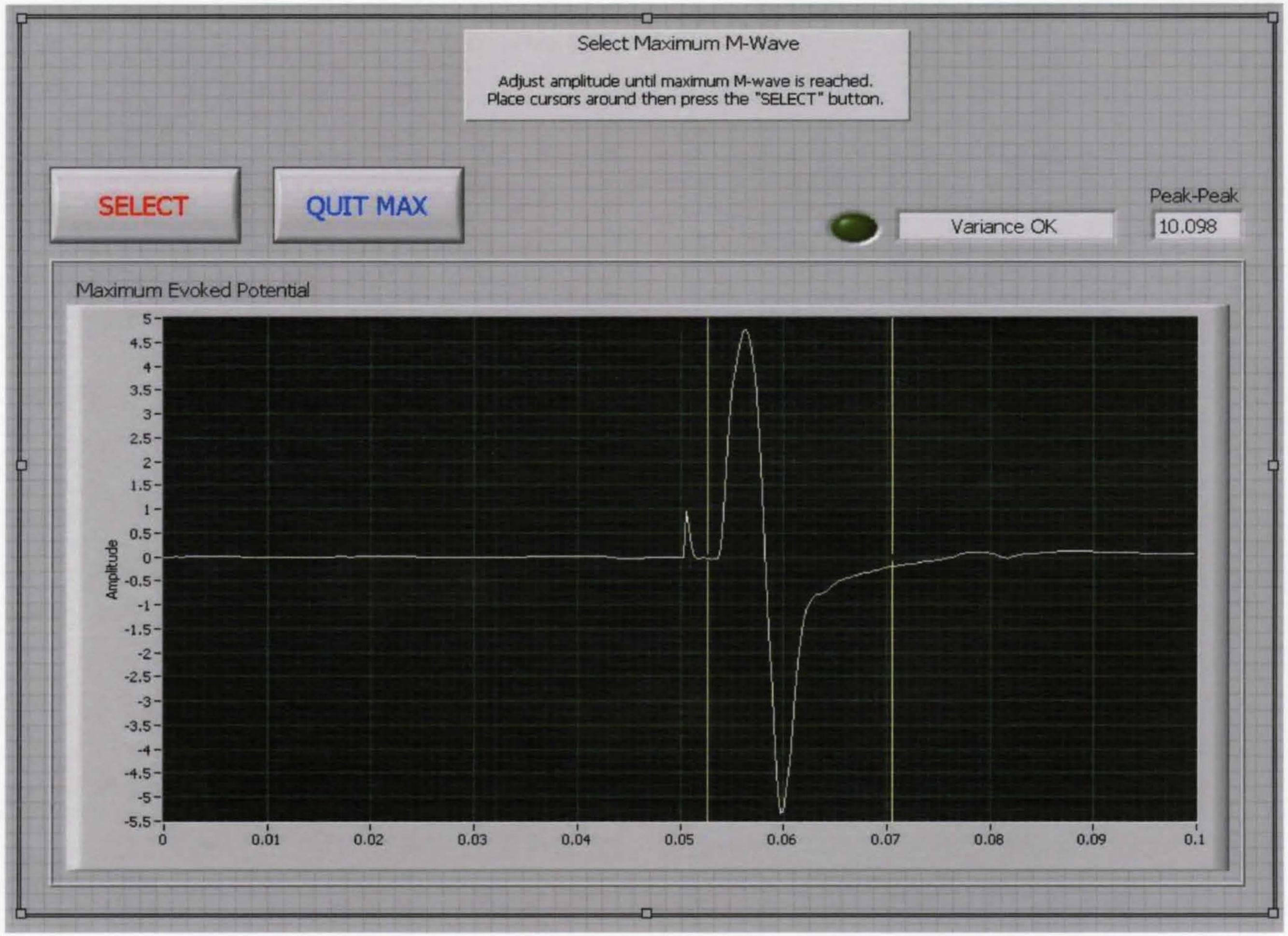

Figure 4.8. Maximum Evoked Potential Window in LabVIEW program

It was decided that the MEP be collected first during the experiment for several reasons noted by Cavasin (1989) and others. The MEP collection is the most uncomfortable part of the experiment and collecting it first allows subjects to relax during the lower stimulus amplitudes used for collecting the sub-maximal M-waves. Moreover, collection of the MEP allows for the post-stimulus window length to be defined accurately. An optimal post-stimulus window length is one that is long enough to collect the entire duration of the M-waves but short enough to limit noisy tails that may interfere with pattern recognition later. The MEP defines the largest necessary post-stimulus window length and collecting it first reduces tail end noise during sub-maximal M-wave collection. The MEP collection also enables the operator to easily detect a poor recording electrode or stimulating electrode placement. The placement can then be corrected before the M-waves are recorded.

4.2.4.2 Sub-maximal Collection

When the MEP has been selected, the program returns to the main window shown in Figure 4.3. The operator then selects START MUAP COLLECTION to begin collecting sub-maximal M-waves. As the operator gradually increases the stimulus amplitude, the raw data responses are displayed by the LabVIEW program in the graphs shown in figure 4.3 (A). Each response is subject to the 60 Hz noise reduction and if the variance check is passed, stimulus artifact elimination and baseline correction are done before the M-wave features are extracted. The current noise reduced response is displayed in the window of Figure 4.3 (B). The extracted features are used to determine whether the response is a new M-wave template or whether it belongs to a previously defined template. The details of this classification are presented in Figure 4.5 and discussed in subsequent sections. Once 3 recorded M-waves are found to belong to the same template, they are averaged and the template is displayed in the center display window superimposed on the live data collection as shown in Figure 4.3 (B). Additionally, the templates are displayed in the template windows along the right side of the program panel as shown in Figure 4.3 (C). The template windows are equipped with counters to show the number of recorded M-waves contributing to that template.

The collection of sub-maximal M-waves is a careful process. Thus, a knowledgeable operator is required to run the LabVIEW system. The operator begins sub-maximal M-wave collection by leaving the stimulus amplitude below threshold such that several instances of the baseline may be detected. The stimulus amplitude is then gradually increased or decreased so that several instances of each level of the CR are collected. An experienced operator is careful not to miss any levels of the CR.

The graphical displays on the LabVIEW front panel are designed to aid the operator in determining the CR increments. Especially helpful are the displays of the templates both in the template windows shown in Figure 4.3 (C) and the center display shown in Figure 4.3 (B). Using these displays, the operator can determine if more instances of a given template need to be recorded or whether any repeatable M-waves between existing templates are missing.

4.2.5 M-Wave Classification

The pattern classification makes use of Fourier or wavelet coefficients and serves to cluster M-waves produced by identical MU firing combinations. Due to additive noise, a given combination of firing MUs may not produce identical M-waves. The scheme shown in Figure 4.5 effectively decides when M-waves are sufficiently similar to assume they result from the same MU firing combination. As described above, all responses are subject to signal processing before classification.

When a new response is collected it may be the result of a unique MU firing combination or it may be the result of a MU firing combination that occurred to give a previous response. Uniqueness is determined in one of two ways. The first method makes use of the spectral coefficients obtained through the Fourier transform. The spectral coefficients of the newly recorded waveform are compared to the coefficients of all the previously recorded waveforms using a Euclidean distance measure. In the LabVIEW program all coefficients (typically 128 coefficients were calculated as explained above) are used in the distance measure. The Euclidean distance is given by

$$D_E = \sqrt{\sum_{i=1}^{N} [C_R(i) - C_P(i)]^2}$$

where, N= number of coefficients

$C_R(i)$ = features (either spectral or wavelet) of new response

$C_P(i)$ = features (either spectral or wavelet) of previous recorded response

If the Euclidean distance between a new response and a given previous response is less than a certain discrimination threshold, the new response is similar enough to that previous response to assume they both result from the same MU firing combination. The new response is then averaged with the previous response and the result is saved in a storage array. If the Euclidean distance is larger than the discrimination threshold for all previously recorded responses, the new M-wave is deemed unique and is saved in a separate storage array. The discriminating threshold is discussed further in Chapter 5. A template is created when an array storing similar responses contains 3 M-waves. Responses collected later that match a certain template are included in the average. Templates are displayed along the right side of the program window as shown in Figure 4.3 (C).

The second method of classification is identical except that wavelet features are used in place of spectral coefficients. The LabVIEW program makes use of the Daubechies 4 wavelet transform and all coefficients from a 3-level decomposition are used in the distance measure. When wavelet features are selected, the discriminating threshold is different from that in the power spectral analysis. Further exploration of appropriate wavelet transforms and decomposition levels was performed off-line in MATLAB and is discussed in Chapter 5.

4.2.6 Program Termination

The data collection may be terminated at any time by the user. The operator can press the STOP button as shown in Figure 4.3 (A) to stop the stimuli and the recordings.

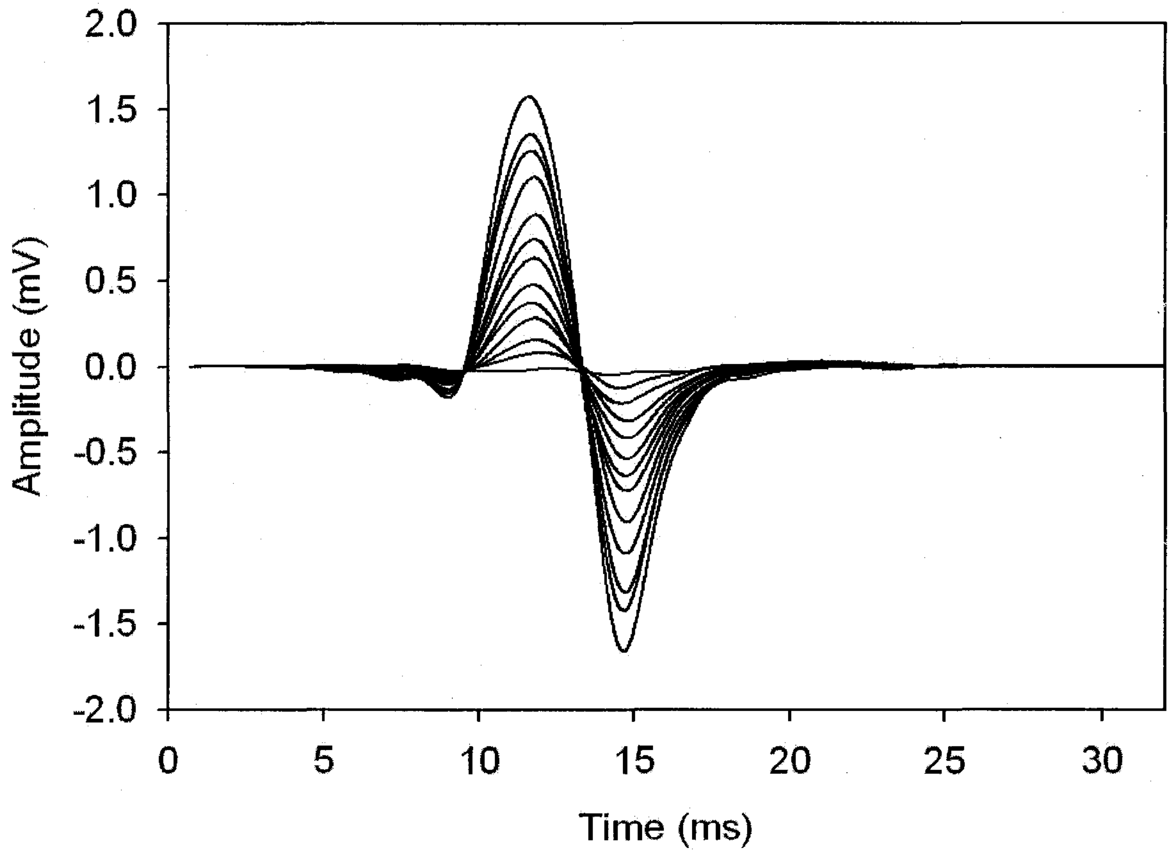

Figure 4.9. Composite response including first 20 MUs recorded from a human thenar muscle

Alternatively the program terminates automatically once 20 templates have been created. Figure 4.9 shows an example of 20 templates created during a recording session.

4.2.7 Storage

When the LabVIEW program terminates, several files are created to store the results of the recording session. The files are in .xls format so that they may be opened in Microsoft Excel. The first output file contains all the raw data signals that were collected during the recording session. This file is important as it can be used for post-processing with the MATLAB algorithms. In this way, different signal processing techniques and feature extraction sets can be tried on the same data and a valid comparison made.

Additionally, a file is created to store the processed M-waves that contribute to each increment of the CR. The M-waves corresponding to the same increment in the CR are averaged to form the templates. Another .xls file stores only the templates. This file contains a header describing the number of M-waves that were averaged to form each template. Finally, the MEP that was selected by the operator at the start of the experiment is saved in .xls format.

CHAPTER 5
M-WAVE PATTERN RECOGNITION

5.1 Introduction

A study was conducted using the left and right thenar muscles of 2 healthy males and 4 healthy females, age ranging from 21 to 60. The objective of the study was to evaluate the aspects of wavelet pattern recognition as a successful classification scheme for M-waves. Moreover, the study was used to investigate the effects of a characteristic discriminatory threshold to be used for all subjects in either the wavelet or power spectral pattern recognition techniques. Though this threshold must be different for different feature extractors, the issues surrounding the choice of a characteristic threshold to be applied universally are the same.

5.2 Evaluating and Comparing M-wave Pattern Recognition Schemes

To accurately evaluate and compare wavelets and power spectral coefficients as feature sets in M-wave pattern classification, it is first necessary to define the characteristics of an ideal classifier for this particular data. A successful M-wave pattern recognition scheme is one in which all true M-waves are extracted without creating clusters of additional signals that are not unique M-waves, but M-waves plus noise. A classifier that is insensitive will place different M-waves in the same cluster resulting in an underestimate of the true number of M-waves. However, a classifier that is too sensitive will fail to cluster signals that represent the same M-wave and differ only by a variation in additive noise. This classifier will overestimate the number of M-waves. As the number of M-waves is a key component in MUNE calculations, it is essential for a reliable clinical diagnostic technique that the number of calculated M-waves represents the true number of unique M-waves recorded from the patient.

The aim of this thesis is to investigate the sensitivity of an M-wave classifier using different feature sets. The goal is to draw a comparison for different feature sets for M-wave pattern classification so as to determine which set best extracts the true M-waves. However, the success of a classifier does not solely depend on the feature set used. The feature set merely isolates the characteristics used to evaluate the different M-waves. These characteristics must be separable. The discriminator, in this case, a Euclidean distance threshold value, is the means to separate the M-waves based on the extracted features. For this reason, the work presented here includes an analysis of the discriminatory threshold values alongside the different feature sets. Furthermore, the response of the different feature sets to different discriminatory threshold values is used as a measurement for the applicability of that feature set to M-wave pattern recognition as described further below.

5.3 Motivation for a Characteristic Discriminator

In practice, different subjects yield quite different M-waves during a data recording. This is due to anatomical differences between subjects and also variations in electrode placement as described in Section 2.2. Thus, for a given feature set, optimal discriminatory thresholds will vary from subject to subject.

There are advanced techniques to train classifiers to produce an automated system with a threshold discriminator optimized for each subject. However, these techniques are not practical for the experiments outlined here and for clinical MUNE. The reason for this is that the algorithms for training a classifier require approximately double the amount of data, due to the additional signals required for the training. This process is time consuming and affects a subject's comfort. In clinical MUNE these are important drawbacks because a physician generally favours diagnostic tests that are efficient. In addition, a subject often experiences difficulty remaining still and calm for additional electric stimuli. In this case, there is increased chance that the subject may change position causing either the stimulating bar or the recording electrodes to move slightly thus, recruiting and recording a different distribution of MUAPs. The effects of electrode placement on surface recordings were described in Section 2.2. An agitated patient may also experience increased levels of background EMG. This adds significantly to the noise in M-wave recordings.

Adding further to the drawbacks of a trained M-wave pattern classifier are the physiological implications of additional stimuli. Continuous stimuli alter the ionic concentrations in the body tissues after a prolonged period of time. This affects the strength of stimulus needed to generate an AP and additionally could introduce latency shifts in the recorded signals as discussed further in Section 5.10. Changes in blood supply also occur and this effectively alters the field distribution for the body tissue in the vicinity of both the stimulating and recording electrodes. Thus, it is imperative that MUNE is performed with a minimum number of applied stimuli.

The reasons stated above motivate the need for a universal discriminatory threshold value regardless of the method used to extract M-wave features. In the previous automated MUNE techniques, described in Section 2.6, M-wave pattern classification was carried out using power spectral coefficients as the feature set and a Euclidean distance measure with an empirically determined universal discrimination threshold. However, no detailed investigation as to the effects of the empirically determined threshold was performed and there is no justification presented in the literature for the chosen value.

In this thesis, a thorough examination of the M-wave data is performed to find a universal discriminatory threshold that gives the most accurate results over the largest subject range when used with a given feature set. Although each feature set will require a different characteristic discriminatory threshold, comparisons can be drawn between feature sets based on their relative sensitivity to the threshold. An ideal feature set will be one that yields the same number of M-waves over a range of discriminatory threshold values. This ensures that if the optimal discriminatory threshold for a given subject is different than the chosen universal threshold, the resulting M-wave number will not be significantly altered, thus the MUNE will remain accurate. For feature sets demonstrating high sensitivity to discriminatory threshold, subjects with optimal thresholds different from the universal threshold will have inaccurate M-wave numbers. The clinical issue then is that the MUNE will be imprecise and an erroneous diagnosis may be made.

The remaining sections of this chapter outline how a universal discriminatory threshold was determined for each of the feature sets examined in this thesis. In addition, a comparison of the different feature sets is made using threshold sensitivity as a measure for success.

5.4 Threshold Determination

The investigation into the response of feature sets to discriminatory threshold values was carried out with the MATLAB routines described in Section 4.2.3 on previously stored data collections. However, an initial estimate of the best universal discriminatory threshold was necessary to first collect the data using the real-time LabVIEW program. Although it is the raw data collected by the LabVIEW program that is used for post-processing, the discriminatory threshold enabled the creation of M-wave template displays during the experimental data collections. The template displays on the LabVIEW program were responsible for aiding the operator in controlling the stimulator to ensure that all occurring M-waves were captured. Thus, the data collected from the 6 subjects was collected using a rough estimate of the ideal universal discriminator merely for the purpose of aiding the operator. This rough estimate of the universal discriminator also gave a starting point when investigating the threshold sensitivity of the different feature sets with MATLAB as described in Section 5.6.

The rough estimate of the universal discriminatory threshold was determined empirically using three subjects' data collected in real-time with the LabVIEW program created for this thesis. The LabVIEW program was set to FOURIER and the parameter "Threshold" was set to an arbitrary low value. These parameters are seen on the LabVIEW program front panel in Figure 4.3. With the aid of an experienced MUNE operator the sub-maximal collection began. The operator used the displays provided with the LabVIEW interface shown in Figure 4.3 to determine whether the automated classification scheme was classifying the recorded sub-maximal M-waves correctly.

At extremely low threshold values, the design of the LabVIEW program resulted in the number of determined templates to be low. This is because the low discriminatory threshold makes the classifier very sensitive. Thus, most recorded signals were not found to match any of the previous recorded signals because the Euclidean distance between them was greater than the discriminatory threshold. Since the LabVIEW program requires a minimum of three signals clustered together before the definition of a template, very few templates were created. If the operator determined that the automated classifier was identifying too few M-waves at a low discriminatory threshold the collection was halted and the threshold parameter increased slightly.

As the threshold parameter increased the number of M-wave templates determined by the LabVIEW program increased also. The operator collected, halted, increased the threshold and re-started sub-maximal collection until the number of M-wave templates determined by the LabVIEW program began to decrease. This decrease occurred because the discriminatory threshold reached a value too high, making the classifier insensitive. In this case, the Euclidean distance between recorded waveforms was often less than the discriminatory threshold and the waveforms were clustered together in fewer inaccurate groups. The process was then repeated with the LabVIEW program set to WAVELET. Recall from Section 4.2.3.6 that the LabVIEW interface applies a Daubechies 5 3-level wavelet decomposition. The results for the three subjects over the varying discriminatory threshold values are shown in Figure 5.1. The rough estimate of the universal threshold for each of the two feature sets was calculated by determining the range of thresholds for each subject that gave an M-Wave number within

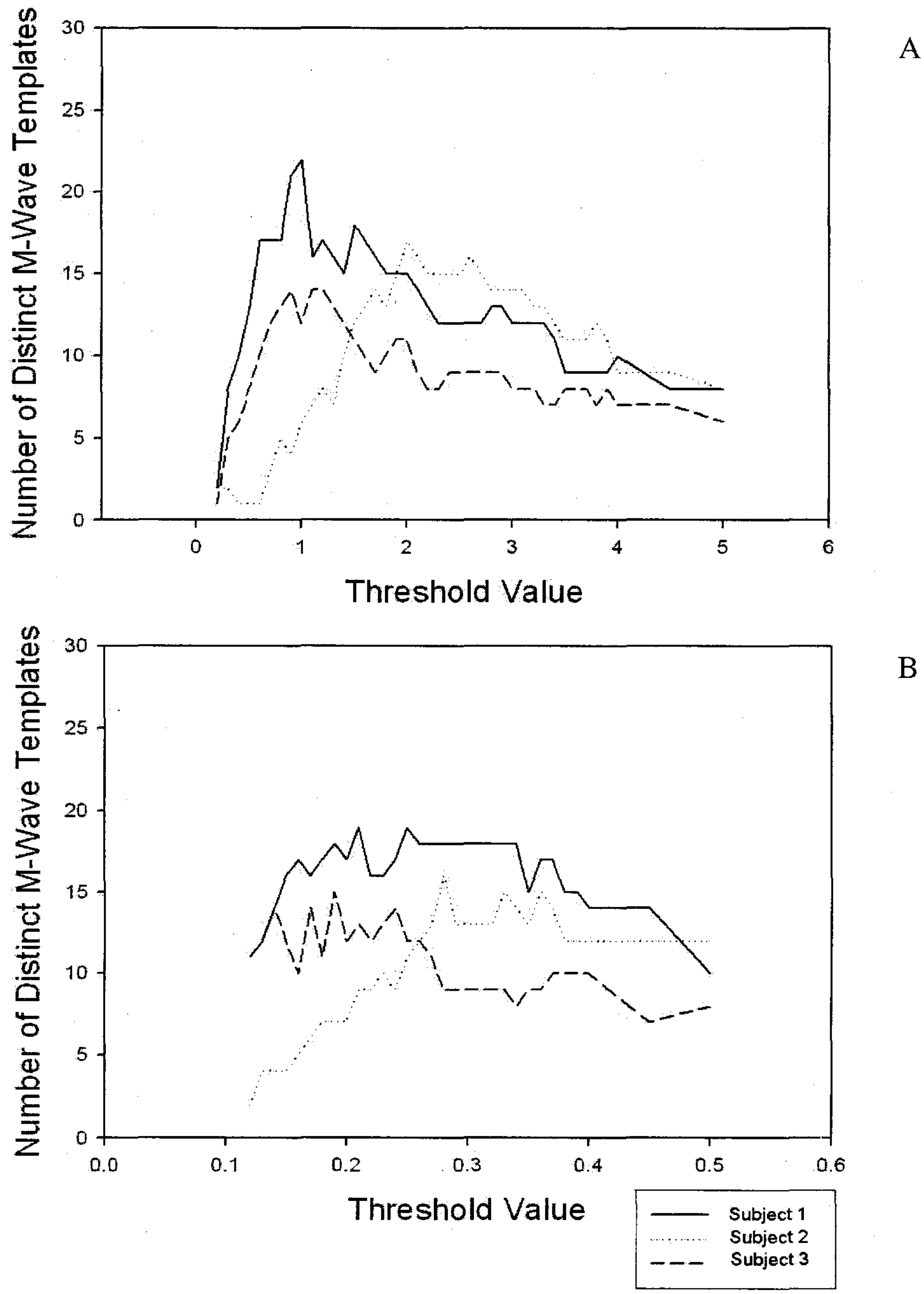

Figure 5.1. Recorded M-wave template number for 3 subjects over varying discriminatory thresholds (A) power spectral (B) wavelets

20% of the maximum M-wave number. The middle of this range for each subject was then taken and averaged with the middle of the range for the other subjects to determine a rough universal discriminatory threshold value. The results were a universal discriminatory value of 1.52 when power spectral features were used as the feature set and a universal discriminatory value of 0.26 when wavelet features were used as the feature set. These thresholds were then used to aid the operator in data collections for the 6 subjects presented in this thesis.

5.5 Choice of the Wavelet Transform

In Section 3.4, the wavelet transform is discussed and a variety of mother wavelets are mentioned. The LabVIEW program and the offline MATLAB algorithms in this thesis, make use of a mother wavelet from the Daubechies family with the depth of decomposition being three levels. This wavelet family and decomposition level combination is commonly used in MUAP feature extraction (Zhou and Rymer, 2003, Hu and Wang, 2004). However, there are several other justifications for this choice of wavelet.

First, recall from Section 3.4 that the wavelet transform is by definition a correlator. The transform correlates the signal with scaled and shifted versions of the mother wavelet. When the signal and the wavelet overlap, the coefficient will be large. When the signal and the wavelet are distinct the coefficient will be small. Thus, an ideal wavelet, one that will yield the largest coefficients when correlated to the signal, is one that has similar characteristics to the signal with respect to smoothness, symmetry and

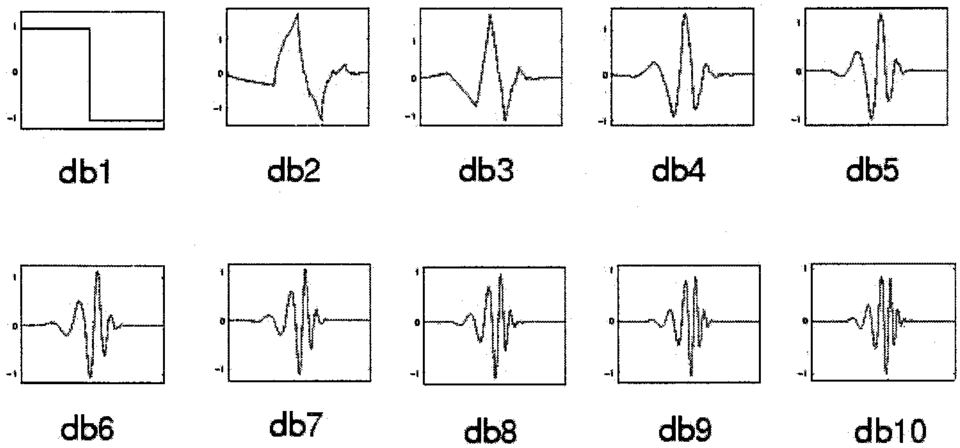

Figure 5.2. Daubechies family of mother wavelets (Matlab Version 7.0 help files)

phases. Figure 5.2 shows a plot of the Daubechies family of mother wavelets. As seen from this figure, the Daubechies 2 mother wavelet has similar characteristics to the maximum M-wave. However, due to alternation, only a limited number of unique M-waves can be recorded. As these are generated by the activity of only a few MUs, it is intuitive that the correlator should more closely match the characteristics of MUAPs then those of the maximum M-wave. Thus, the Daubechies 5 mother wavelet was chosen for the offline MATLAB analysis because it allows for high correlation at the correct shift and scaling values for the low amplitude M-waves. The Daubechies 4 mother wavelet was chosen for the real-time LabVIEW system for simplicity. The LabVIEW software has a built in Daubechies 4 transform but not a Daubechies 5 transform. Moreover, as presented in Section 5.8, the results for M-wave pattern classification are the same for both Daubechies 4 and Daubechies 5 mother wavelets. For these reasons, it was decided that Daubechies 4 would generate sufficient results for real-time data collection.

The wavelet transform in both the MATLAB algorithms and the LabVIEW software were implemented using a dyadic approach with the Mallat algorithms as explained in Section 3.4. The number of decomposition levels for this algorithm was determined based on a frequency characteristic analysis of the M-wave data. An algorithm was programmed to calculate the power spectral density for the entire set of recorded M-waves from each subject. The power spectral density measurement was made by taking the Fourier transform of each M-wave in the data set then averaging the coefficients of all M-waves at each frequency. The result for a set of M-waves collected from 1 of the 6 subjects is shown in Figure 5.3. This figure shows the frequencies within the M-waves corresponding to the greatest power. These frequencies are where the information or features of the signal exist and this is what must be captured by the M-wave pattern classifier. Figure 5.3 also shows the sub-bands captured in the approximation and detail coefficients during the Mallat decomposition process. From here, it is evident that the majority of the M-wave signal power and hence, signal information, is captured in the third level approximation and detail coefficient vectors. Therefore, the standard LabVIEW and MATLAB algorithms created for this thesis use a 3-level decomposition. Section 5.8 provides a further investigation into the choice of mother wavelet and decomposition level and the effect this has on M-wave pattern recognition.

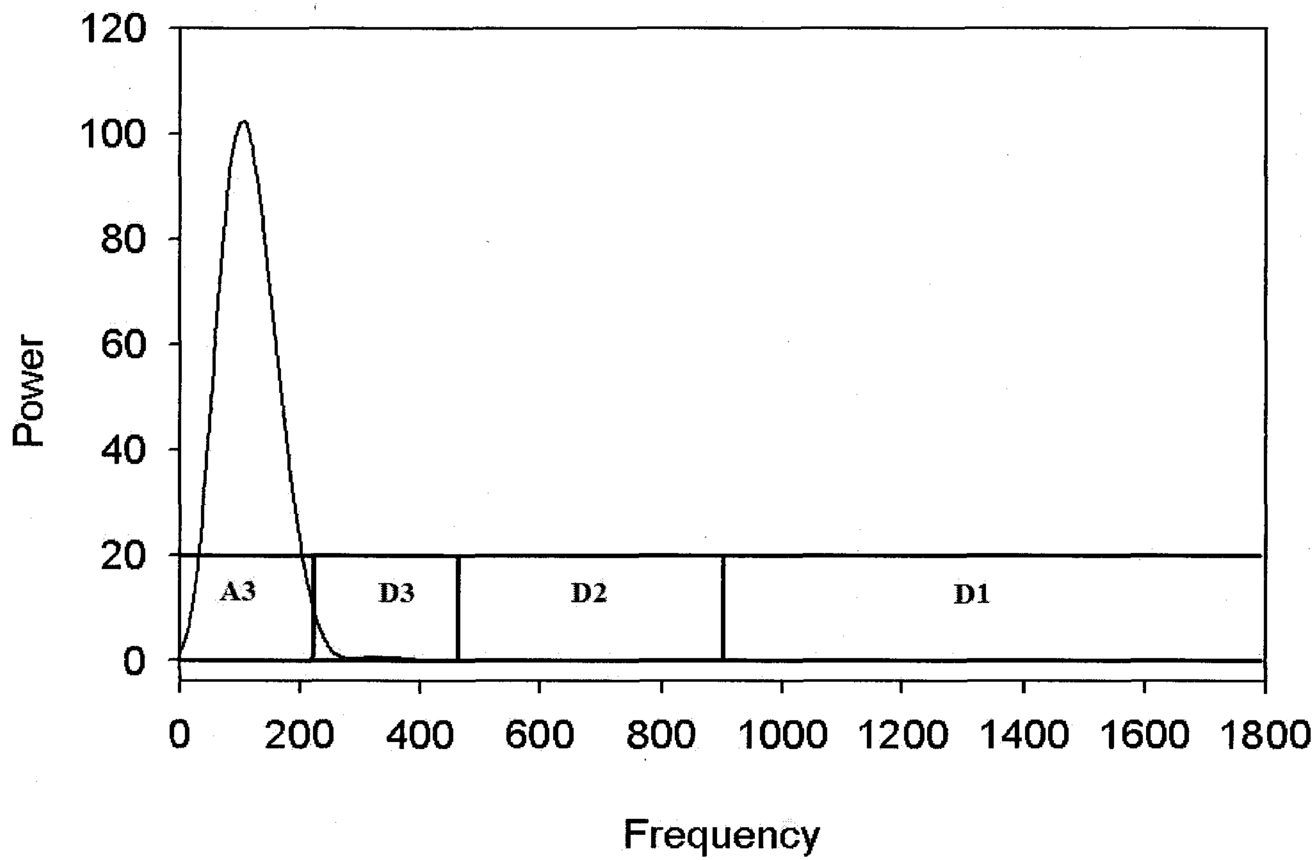

Figure 5.3. Power spectral density for subject A with wavelet decomposition frequency bands

5.6 Comparison of Power Spectral and Wavelet Features

As described in Section 5.3, the use of the wavelet transform for feature extraction in M-wave pattern recognition can be compared to the traditional power spectral features by looking at the sensitivity of the feature set to threshold changes. As stated above, the more applicable a feature set is to M-wave pattern recognition, the less sensitive it will be to threshold variations.

The raw data collected from 6 subjects by the LabVIEW program was used to calculate threshold sensitivity for both the wavelet and spectral feature set. For each subject, the collected responses were subjected to the post-processing MATLAB algorithms. As mentioned in Section 4.2.3 the MATLAB program simulates the real-time LabVIEW interface but operates on previously recorded data. This enables different system parameters to be applied to the same data set. Each subject's collected data was passed through the MATLAB program multiple times, each pass using a different threshold discriminator. For each value of the discriminatory threshold, the number of automatically determined M-waves was saved. For both wavelet and spectral feature sets the set of rough estimate of the universal discriminatory threshold, found as described in Section 5.4, was used as a starting point. The MATLAB program was designed to use 10% of the rough threshold estimate as an increment number, then increase and decrease the rough threshold estimate by multiples of this increment calculating the number of M-waves for each unique value. The results for 1 of the 6 subjects are shown in Figure 5.4 and represent the typical case. Note that the data in Figure 5.4 (B) was created using a 3-level Daubechies 5 traditional wavelet decomposition. Although power spectral and wavelet features require thresholds that are quite different, both show the same general trends in M-wave number over threshold changes. Figure 5.4 shows there exists a maximum number of M-waves at a distinctive threshold value. From the discussion in Section 5.4 a discriminatory threshold that is either too low or too high will yield an M-wave number that is lower than the true number. To further examine this property, successive subtractions of the set of unique M-wave templates obtained with the largest number of members was carried out. That is, each M-wave template is subtracted from the next largest. If the pattern recognition is correct the resulting waveforms should all have the shape of MUAPs. If the number of templates in the CR is too large some of the resulting signals would just be additive noise. The analysis for all subject results showed that no resultant waveforms resembled noise. Thus, it is reasonable to assume that the discriminatory threshold value that generates the largest number of M-waves is the most accurate for that given data set. For the remainder of this thesis, the term characteristic threshold is used to describe the threshold at which the maximum number of M-waves occurs for individual subjects. When the numbers of M-waves at each threshold are averaged over all subjects, the threshold at which the average maximum M-wave occurs is termed the average characteristic threshold.

The M-wave numbers for all subjects at each threshold were averaged to produce Figure 5.5. This figure shows that the average M-wave number for both wavelet and power spectral features has a specific maximum. As discussed earlier it is reasonable to use the threshold at this maximum as a characteristic discriminatory threshold for all subjects when performing real-time M-wave pattern recognition with either power

A

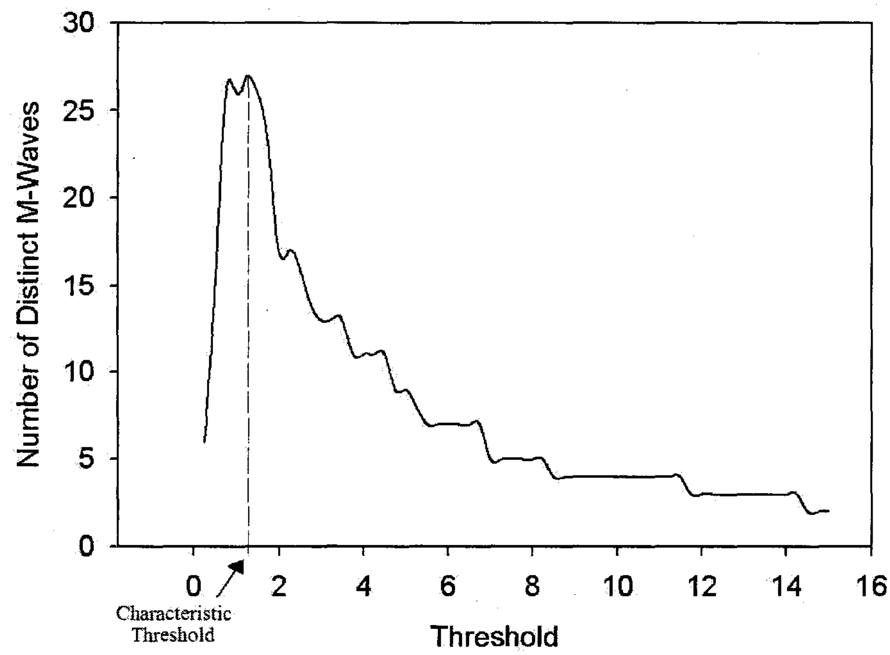

B

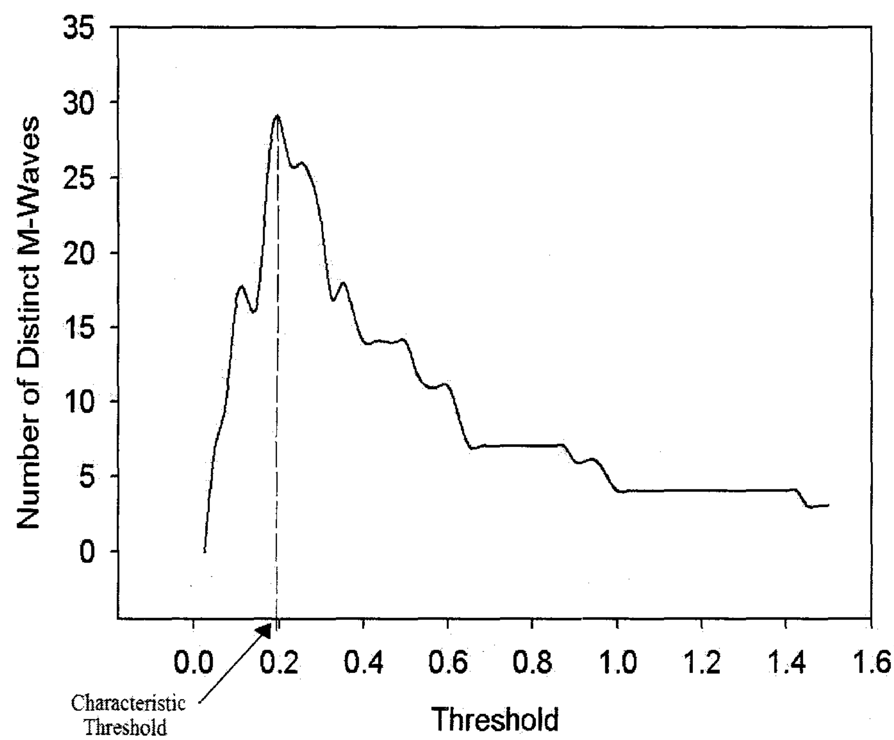

Figure 5.4. Variations in M-wave number for one subject for (A) power spectral based features (B) wavelet based features

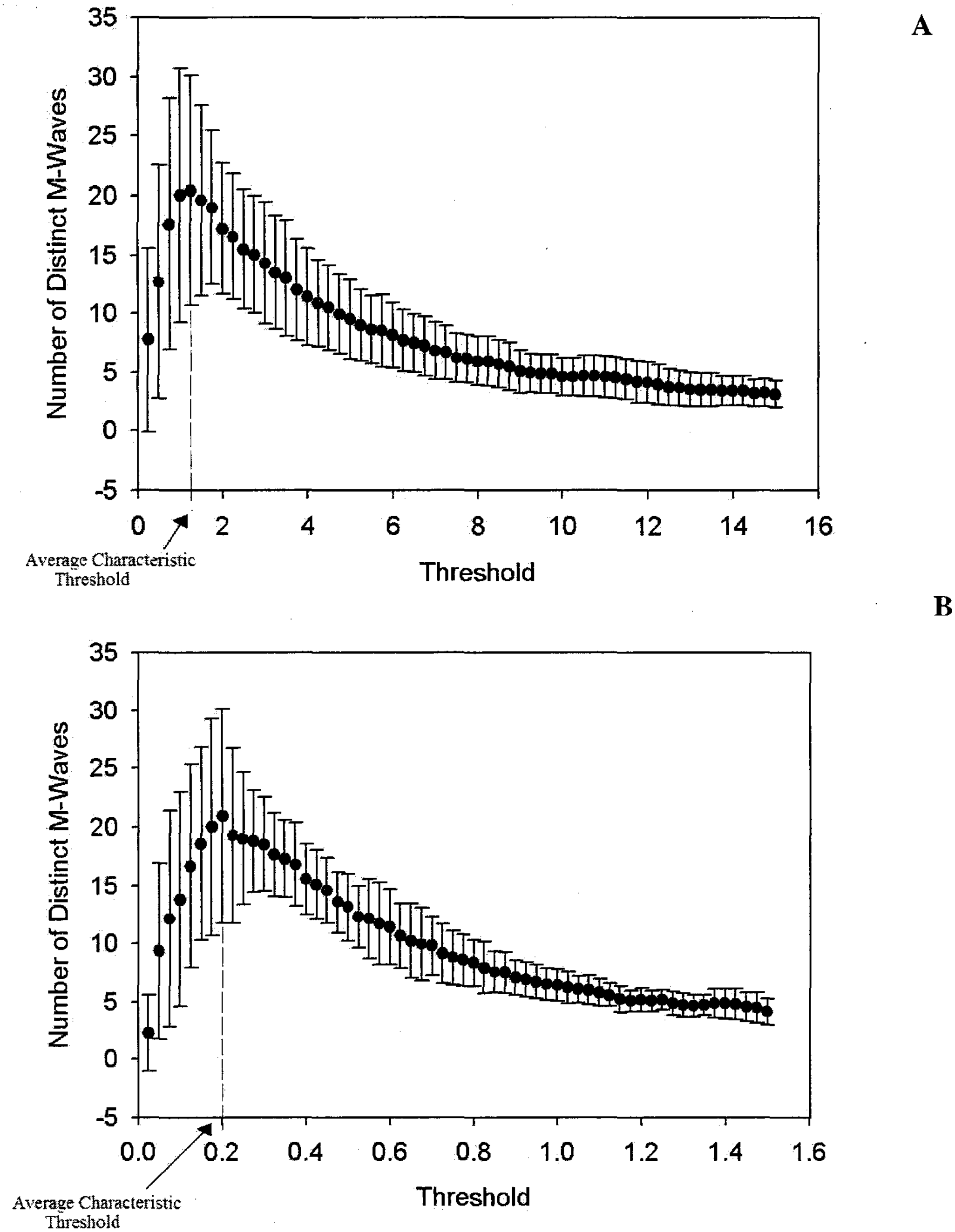

Figure 5.5. Average and standard deviation M-wave number for varying thresholds for (A) power spectral based feature set (B) wavelet

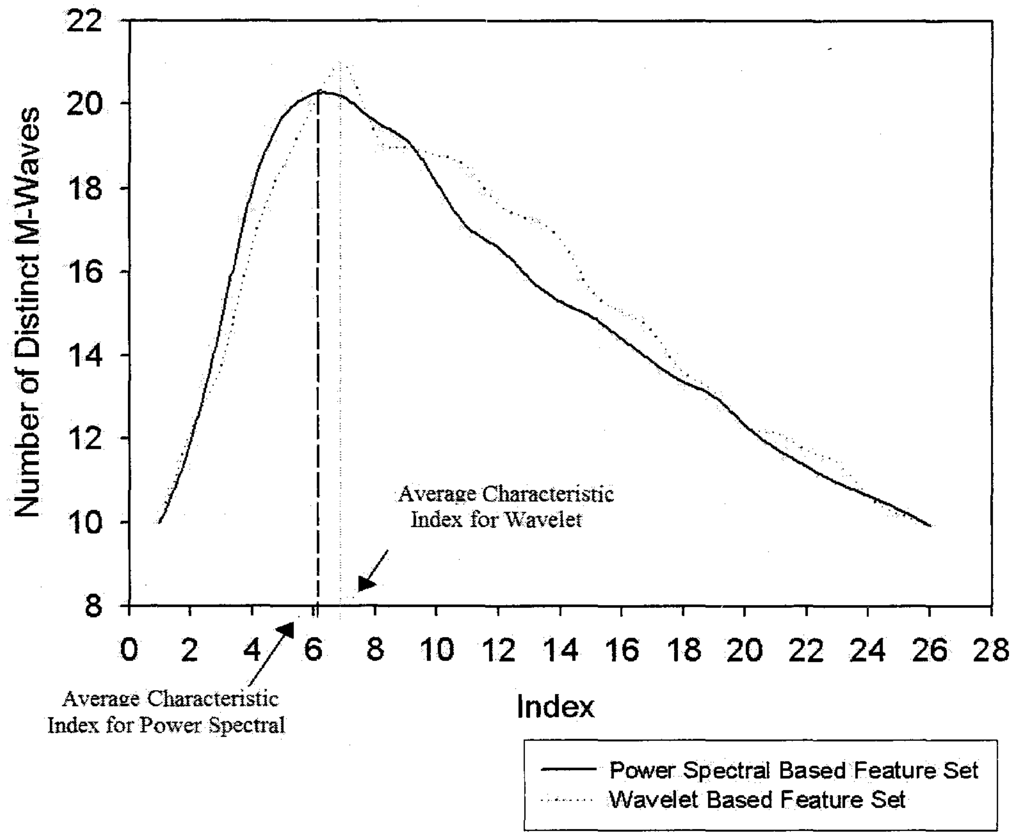

Figure 5.6. Average number of distinct M-waves greater than 10 for power spectral and wavelet based feature extraction

spectral or wavelet coefficients. Ideally, for a clinical system, the results of a large number of subjects would be included to find the average characteristic threshold applicable for real-time data. However, the average characteristic threshold shown in Figure 5.5 is the result of only 6 subjects. For the purposes of this thesis, this is taken to be a sufficient indication of the average characteristic threshold had more subjects been considered.

Because the spectral and wavelet feature sets operate for different thresholds, the plots in Figure 5.5 were manipulated for a meaningful comparison to be drawn. Figure 5.6 shows the average M-wave numbers greater than 10 as derived from both feature sets. In this figure, the number of M-waves is plotted against an index as opposed to actual threshold value such that the results for power spectral and wavelet features may be contrasted. This index is simply determined from the two ranges of threshold values giving M-wave numbers greater than or equal to 10. For the purposes of the following discussion, the index at which the averaged maximum M-wave number occurs for either power spectral or wavelet analysis will be termed the average characteristic index.

Section 5.3 explains that an ideal feature set is one where the maximum M-wave number is least sensitive to threshold changes. Thus, Figure 5.6 can be used to assess how the M-wave number changes, in both power spectral and wavelet based pattern recognition, as the threshold index deviates from the average characteristic index. From Figure 5.6, it is evident that when the threshold index is only slightly deviated from the characteristic index, the power spectral based pattern recognition exhibits only small changes in the maximum M-wave number while the wavelet based pattern recognition shows marked changes. This is shown in Figure 5.7, when the index is varied from the average characteristic index by a value of 2. Table 5.1 summarizes these results, and includes results for when the index is varied by 3, 4 and 5 around the average characteristic index. The results, here suggest that the power spectral feature set is less sensitive than the wavelet feature set to threshold variations.

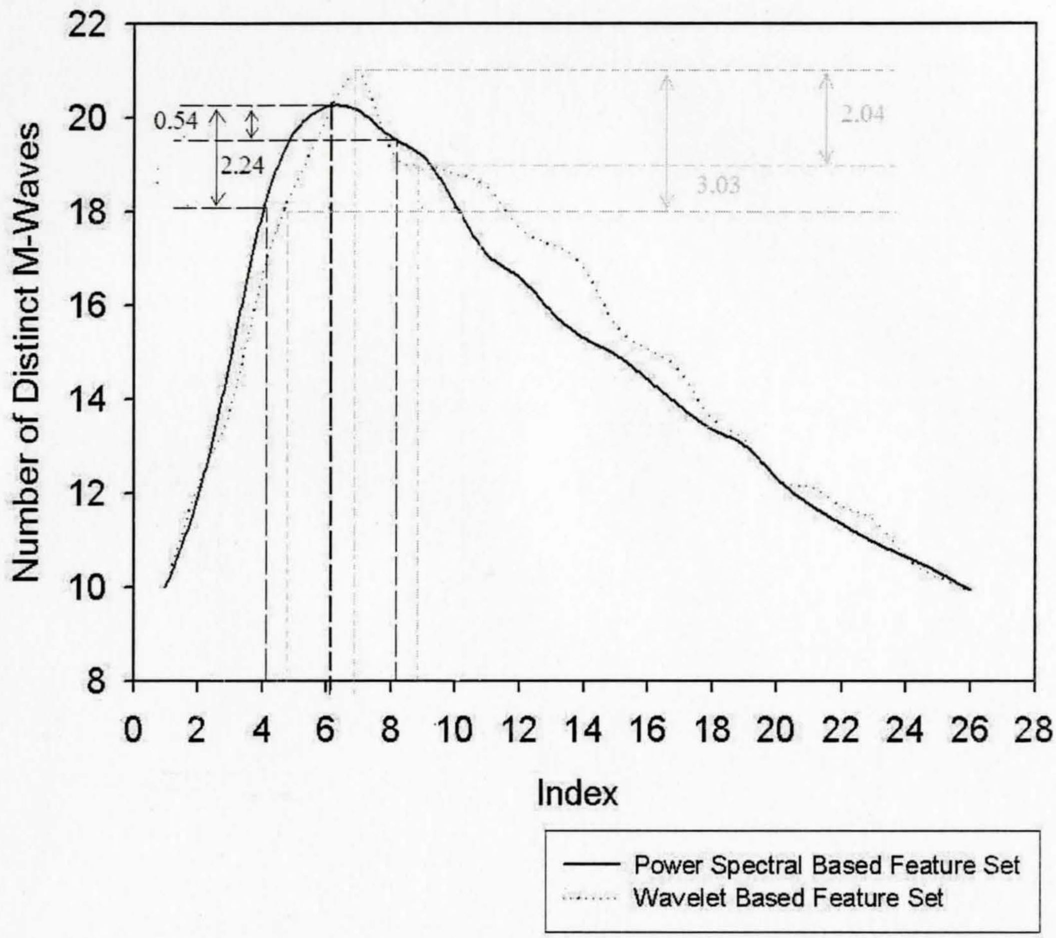

Figure 5.7. Average number of distinct M-waves greater than 10 for power spectral and wavelet based feature extraction with average decrease in number for index variations of 2 from the average characteristic threshold

Table 5.1: Deviations from maximum M-wave number for specific deviations from characteristic index

Index Distance from Characteristic Threshold	Average Decrease in M-Wave Number	
	Power Spectral	Wavelets
2	1.39	2.52
3	1.43	2.61
4	2.27	3.25
5	3.08	3.18

However, this only holds true when the index is varied slightly around the characteristic value. To make accurate judgements about threshold sensitivity, it is first necessary to examine the individual data for each subject to determine typical deviations from the average characteristic threshold. For each subject, the characteristic threshold was found and the distance between it and the average characteristic threshold shown in Figure 5.5 was calculated. Next, the distances for each subject were combined to calculate an average distance from the average characteristic thresholds. Finally, because the thresholds for power spectral and wavelet features are different, the average distance is expressed as a percentage of average characteristic threshold value. This is summarized in Table 5.2.

The average distance between individual characteristic thresholds and the average characteristic threshold for each feature set was then used to determine how the M-wave number changed. For example, when the threshold differed by 0.64 from the average characteristic threshold in Figure 5.5 (A), the average number of M-waves was 5 less than the maximum. Table 5.3 summarizes these results. When all subjects were included, the average M-Wave deviation was just over 20% of the maximum value. Thus, 20% was taken as the maximum acceptable error in M-wave numbers. Figure 5.8 shows the index range for which the M-Wave number is within 20% of the maximum value for both power spectral and wavelet based feature sets. For power spectral based feature sets the M-wave number is within 20% of the maximum for an index range of approximately 8 while for wavelet based feature sets the M-wave number is within 20% of the maximum for an index range of approximately 10. This measure is more significant than those

Table 5.2: Distance between individual and average characteristic thresholds

Subject	Characteristic Threshold		Distance from Average Characteristic Threshold	
	Power Spectral	Wavelets	Power Spectral	Wavelets
Subject 1 (Right Thenar)	3.50	0.58	2.02	0.33
Subject 1 (Left Thenar)	2.25	0.33	0.77	0.08
Subject 2 (Right Thenar)	1.25	0.20	0.23	0.04
Subject 2 (Left Thenar)	1.00	0.20	0.48	0.04
Subject 3 (Right Thenar)	0.50	0.08	0.98	0.17
Subject 3 (Left Thenar)	0.75	0.13	0.73	0.12
Subject 4 (Right Thenar)	1.25	0.20	0.23	0.04
Subject 4 (Left Thenar)	0.75	0.20	0.73	0.04
Subject 5 (Right Thenar)	1.25	0.25	0.23	0.01
Subject 5 (Left Thenar)	1.75	0.25	0.27	0.01
Subject 6 (Right Thenar)	2.25	0.33	0.77	0.08
Subject 6 (Left Thenar)	1.25	0.18	0.23	0.07
Average distance between individual and average characteristic thresholds:			0.64	0.09
Average distance between individual and average characteristic thresholds as a percentage of universal characteristic threshold:			51.11%	43.08%

shown in Table 5.1 because it takes into consideration the subject variability from the average characteristic discriminatory threshold that is experienced in practice. The measure presented in Figure 5.8 shows that over the range of typical subject variations from the characteristic threshold, the wavelet based feature set provides a more constant M-wave number. This indicates that the third level approximation and detail coefficients from wavelet decomposition provide a feature set for M-wave pattern recognition that is somewhat less sensitive to variations in threshold than a feature set obtained through power spectral coefficients.

Table 5.3: Average variations in M-wave number with threshold

	Power Spectral	Wavelets
Avg distance between individual and average characteristic thresholds Expressed as a percentage of universal characteristic threshold	51.11%	43.08%
Avg decrease in M-wave number at end points of range	4.9	4.93
Avg decrease in M-wave number Expressed as a percentage of maximum M-wave number	24.0%	23.6%

5.7 Intra- and Inter-Class Distances

In addition to threshold sensitivity measurements, wavelet and power spectral feature sets can be compared by examining the intra- and inter-class distances for the M-wave clusters. To perform this measurement, a data set collected from 1 of the 6 subjects was

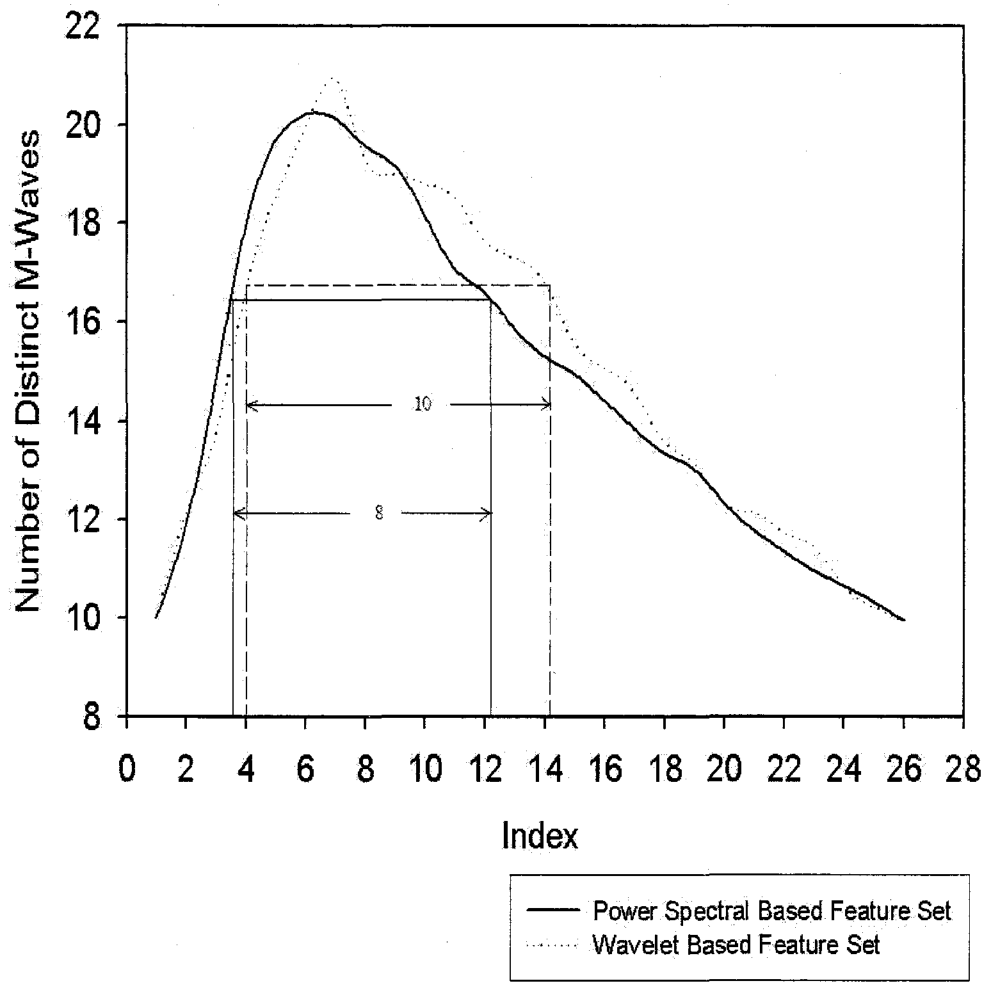

Figure 5.8. Index range for which M-wave number is within 20% of the maximum M-wave number

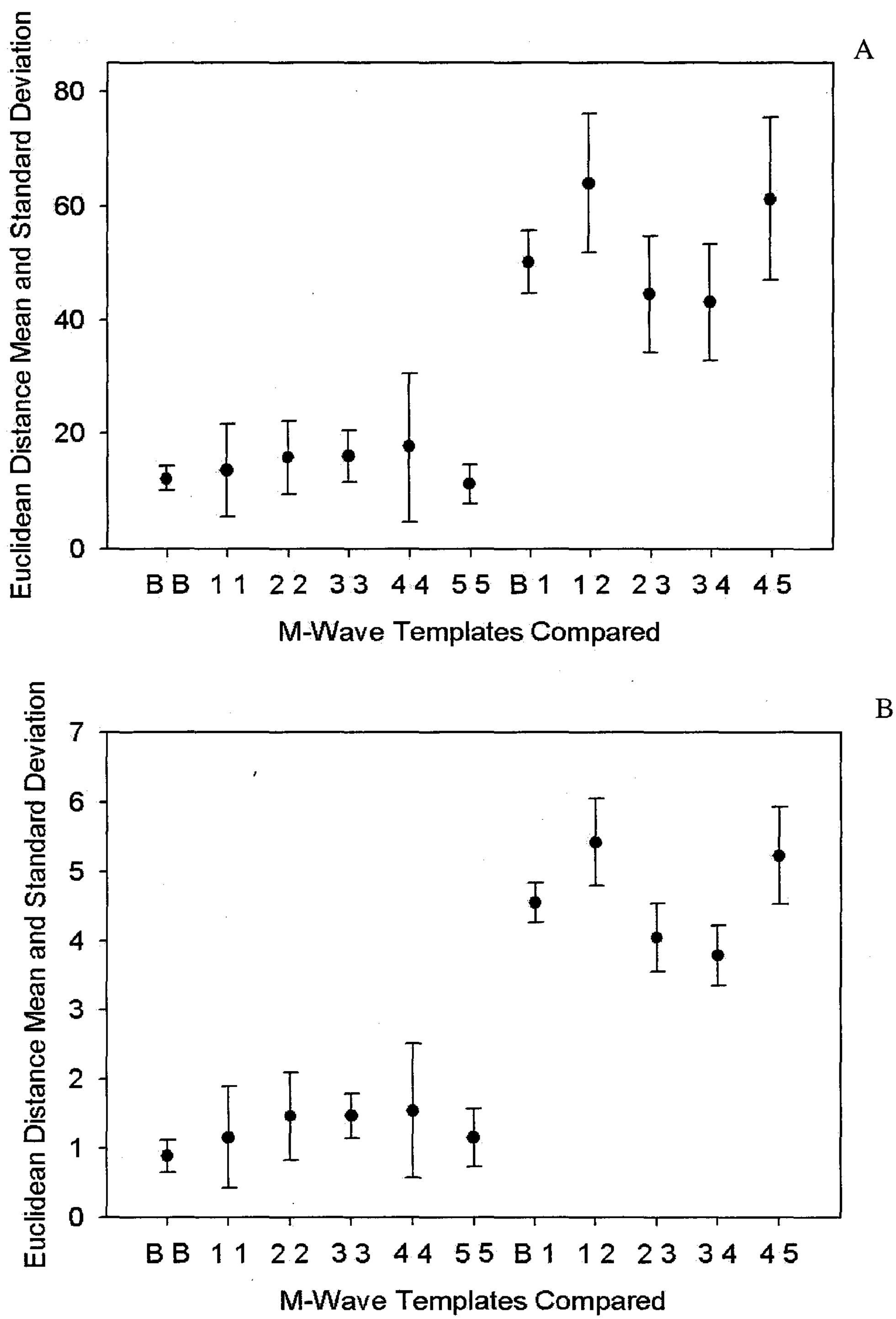

Figure 5.9. Intra-class and inter-class Euclidean distances for the smallest 5 M-wave templates using (A) power spectral coefficients (B) wavelet

visually evaluated and the recorded M-waves were clustered into templates offline, by an experienced MUNE operator. A MATLAB algorithm was designed to extract the features of each M-wave, either through wavelet or power spectral analysis, then calculate the Euclidean distance between the feature sets of M-waves previously grouped in the same cluster, the intra-class distance, and between the feature sets of M-waves previously grouped in different clusters, the inter-class distance. For each template comparison, the calculated intra- and inter-class distances were averaged and the standard deviation calculated as shown in Figure 5.9. For example, the point at BB is the average Euclidean intra-class distance between M-waves classified in the baseline template. The point at B1 is the average Euclidean inter-class distance between members of the baseline template and members of the first or lowest amplitude true M-wave template.

As discussed in Section 5.2, a robust pattern recognition scheme requires that the feature sets be separable. Therefore, the greater the distance between intra- and inter-class average Euclidean distance the more separable are the distinct M-wave templates. Figure 5.9 shows that when power spectral coefficients are used as the feature set, the Euclidean distance between two M-waves of the same class is sometimes close in value to the distances between two M-waves of different classes. This is captured by the overlapping error bars for intra- and inter-class calculations. Contrarily, when the A3 and D3 vectors of a Daubechies 5 wavelet composition are used as the feature set, the intra- and inter-class Euclidean distances are separate. This further demonstrates the improvement in M-wave pattern recognition when wavelets are used for feature extraction. This analysis was not carried out exhaustively, as to do so would be very time consuming and difficult for 200 M-waves, thus the results could be the reverse for another subject.

5.8 Motor Unit Number Estimates

Sections 5.6 and 5.7 establish that wavelet based feature extraction performs better than power spectral based feature extraction in M-wave pattern recognition. However, to verify that the M-waves collected by both pattern classification schemes designed for this thesis are in fact valid, MUNEs were calculated for the 6 subjects. As demonstrated in Chapter 2, MUNE is a well-established technique and there exists a large research database detailing estimates obtained for many different muscles. This database can be used as a comparison for the MUNEs obtained for each subject using the M-wave numbers found by both the power spectral and wavelet feature sets.

Table 5.4: Thenar MUNEs for 6 subjects

Subject	MUNE	
	Power Spectral	Wavelets
Subject 1 (Right Thenar)	145	100
Subject 1 (Left Thenar)	128	49
Subject 2 (Right Thenar)	54	57
Subject 2 (Left Thenar)	112	107
Subject 3 (Right Thenar)	107	102
Subect 3 (Left Thenar)	62	61
Subject 4 (Right Thenar)	90	103
Subect 4 (Left Thenar)	200	177
Subject 5 (Right Thenar)	47	37
Subect 5 (Left Thenar)	76	76
Subject 6 (Right Thenar)	85	78
Subject 6 (Left Thenar)	52	43

Table 5.4 shows the calculated MUNEs for the left and right thenar muscles of the 6 subjects studied in this thesis. These MUNEs were calculated using the equation described in Section 2.4, with an area measurement. The M-wave number used in the equation for each subject was that found when the average characteristic discriminatory threshold from Figure 5.5 was used for both power spectral and wavelet based analysis. Recall from the discussion in Section 5.6 that the ideal characteristic threshold for each subject varies from the average characteristic discriminatory threshold. Thus, for some subjects the M-wave number obtained at the average characteristic threshold is lower than the true M-wave number. This skews the MUNE results. From the equation presented in Section 2.4, a low M-wave number will result in a larger value for the average contribution of a MUAP to the maximum M-wave. Ultimately, this causes a lower than true estimate. Additionally, there are two sources of error associated with the accuracy imposed by the operator. First, the maximum M-wave obtained during the recording session may not have been the true maximum. Secondly, the operator may not have delivered enough stimuli at each amplitude level to capture all the sub-threshold M-waves. These errors, if occurring, also result in a lower than expected MUNE.

From Table 5.5, the average MUNE obtained from the 6 subjects in this experiment is lower than those obtained in other research. As explained, this is attributed to the choice of average characteristic threshold. The experiment outlined in here based the average characteristic threshold on the data from only 6 subjects. A larger study is necessary to determine a truly universal threshold and is beyond the scope of this thesis.

Though the MUNE results for this experiment were low, they were reproducible and as such, the investigation into different feature sets presented in Sections 5.6 and 5.7 is valid.

Table 5.5: Summary of thenar MUNEs in recent studies

Methods	**MUNE Mean ± SD**	**Investigator**
MUAP extraction methods:		
Automated McComas	228 ± 93	Galea et al., 1991
Multiple Point Stimulation, Pk-Pk	206 ± 58	Doherty and Brown, 1993
area	288 ± 95	Doherty and Brown, 1993
Spike Triggered Averaging	135 ± 27	Stein and Yang, 1990
Micro-stimulation	122 ± 38	Stein and Yang, 1990
Manual Incremental McComas	170 ± 62	Stein and Yang, 1990
Automated McComas	198 ± 109	Orsi, 2000
Automated McComas, power spectral	97 ± 45	Salvador (current study)
wavelet	82 ± 39	Salvador (current study)
Force/Acceleration methods:		
Spike-Triggered Averaging, Force	130 ± 39	Stein and Yang, 1990
Micro-stimulation, Force	135 ± 45	Stein and Yang, 1990
Automated McComas, acceleration	122 ± 114	Orsi, 2000

5.9 Alternate Wavelets

In the previous comparison of wavelet features to power spectral features, the wavelet coefficients were the third level approximation and detail coefficients obtained using a Daubechies 5 mother wavelet. This section investigates the wavelet transform as applied to M-Wave pattern recognition, by looking at alternate mother wavelets and decomposition levels for the analysis.

The discussion in Section 5.5 justifies the choice of the Daubechies 5 mother wavelet. This wavelet has similar characteristics to the M-waves. However, as mentioned, the real-time LabVIEW program makes use of the Daubechies 4 mother wavelet for convenience. Figure 5.2 shows that Daubechies 4 and Daubechies 5 differ only slightly in their respective characteristics.

An off-line test was performed to ensure that alternating between these two mother wavelets produced no change in the M-wave pattern recognition. This test consisted of using the off-line MATLAB routines to perform pattern recognition on the data for each of the 6 subjects. The first pattern recognition was performed using a 3-level decomposition with a Daubechies 4 mother wavelet, while the second pattern recognition used a 3-level decomposition with a Daubechies 5 mother wavelet.

Figure 5.10 shows the M-wave number when greater than 10, plotted against an index value to compare the Daubechies 4 and Daubechies 5 mother wavelets when using a wavelet based feature set for M-wave pattern recognition. This comparison is similar to that performed in section 5.6. For reasons justified in Section 5.6, the two feature sets can be compared by examining the index range over which the M-Wave number is within 20% of the maximum value. From the data used to generate Figure 5.10, it is evident that the index range for which the M-wave number is within 20% of the maximum value is 10 for wavelet pattern recognition with the Daubechies 4 mother wavelet and 10 when the Daubechies 5 mother wavelet is used. As expected, the Daubechies 4 and Daubechies 5 mother wavelet are equally sensitive to deviations from the average characteristic threshold.

To further explore the effects of an appropriate mother wavelet, pattern recognition was again performed using the data from the 6 subjects. In this case, the Haar mother wavelet was used in a 3-level wavelet decomposition. The Haar mother wavelet

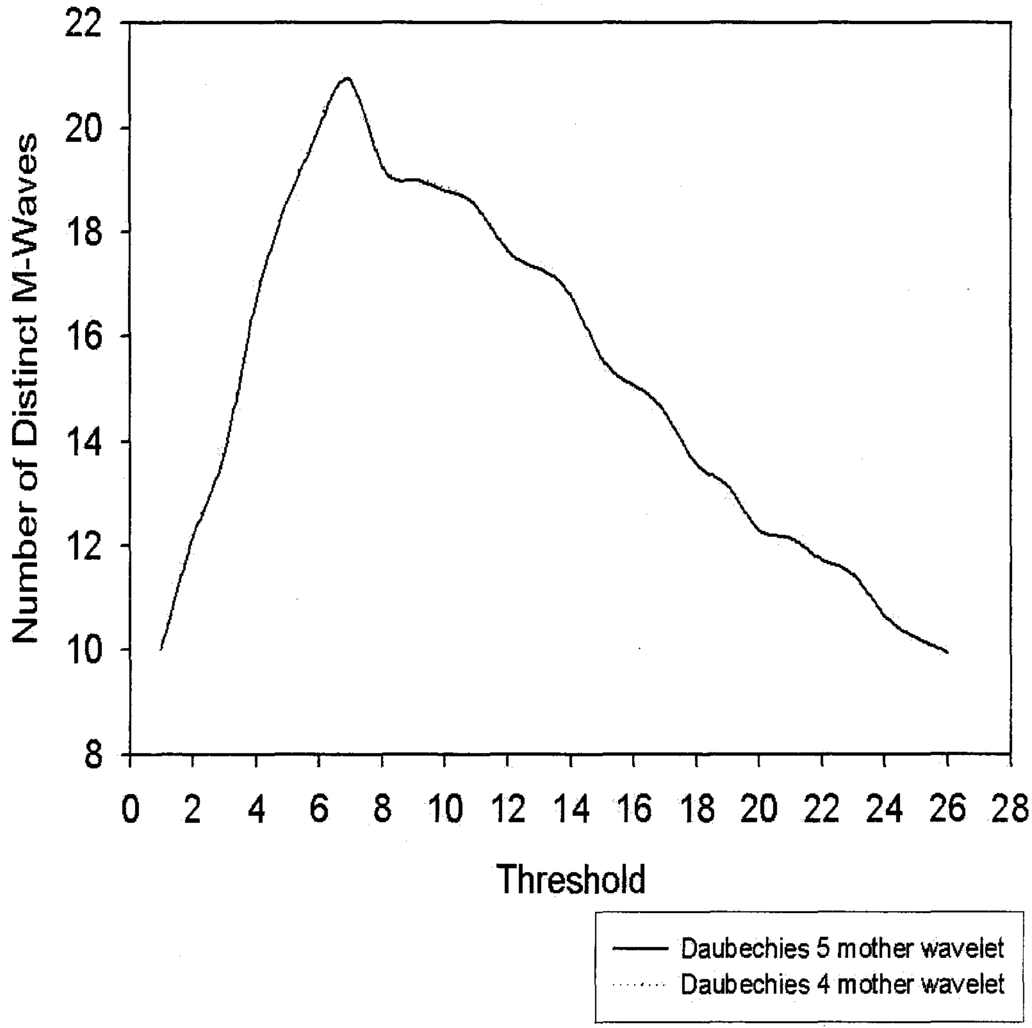

Figure 5.10. Average number of distinct M-waves greater than 10, when using the Daubechies 5 and the Daubechies 4 mother wavelets for feature extraction. The two curves are identical.

is actually the Daubechies 1 mother wavelet and from Figure 5.2 it is obvious that this mother wavelet does not share the same characteristics as the recorded M-waves. For this reason, it is expected that the Haar mother wavelet will not perform as well as the Daubechies 5 mother wavelet in M-Wave pattern recognition. The results of M-wave number over varying threshold indices for both Haar and Daubechies 5 wavelet pattern recognition schemes are shown in Figure 5.11. It is evident that as the threshold varies away from the average characteristic value, the Haar wavelet produces slightly different results than the Daubechies 5 wavelet. For the Haar mother wavelet, the M-wave number is within 20% of the maximum value for an index range of 9, whereas the index range is 10 for a Daubechies mother wavelet. Moreover, a comparison between Figure 5.12 and Figure 5.9 (B) shows that the intra- and inter-class distances are not as separable when a Haar wavelet was used to extract the M-wave features. However, these differences are not pronounced and the two mother wavelets perform similarly. This is because surface recorded MUAPs and M-waves have predominantly biphasic shapes with mostly low frequency content. The ideal mother wavelet should have a shape between that of the Haar and Daubechies 5. A comparison of the Daubechies wavelets in Figure 5.2 and the M-wave responses of Figure 4.9 shows that although Daubechies 2 is basically biphasic it has much sharper features than the M-wave shape and consequently has higher frequency components. The Daubechies 5 mother wavelet has been shown to be very applicable in classifying needle recorded MUAPs which have more complex shapes.

In addition to choice of mother wavelet, the number of levels of decomposition has effects when using wavelets in M-Wave pattern recognition. Section 5.5 justifies the

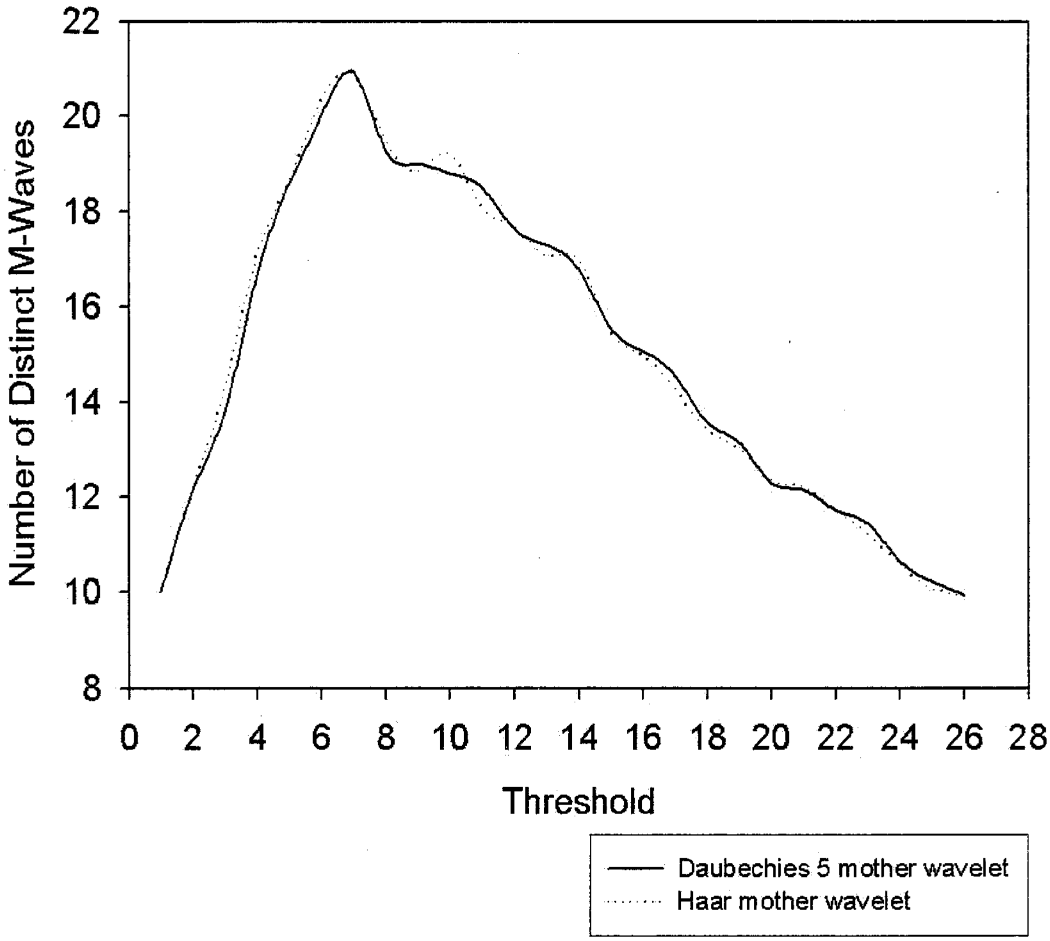

Figure 5.11. Average number of distinct M-waves greater than 10, when using the Daubechies 5 and the Haar mother wavelets for feature extraction

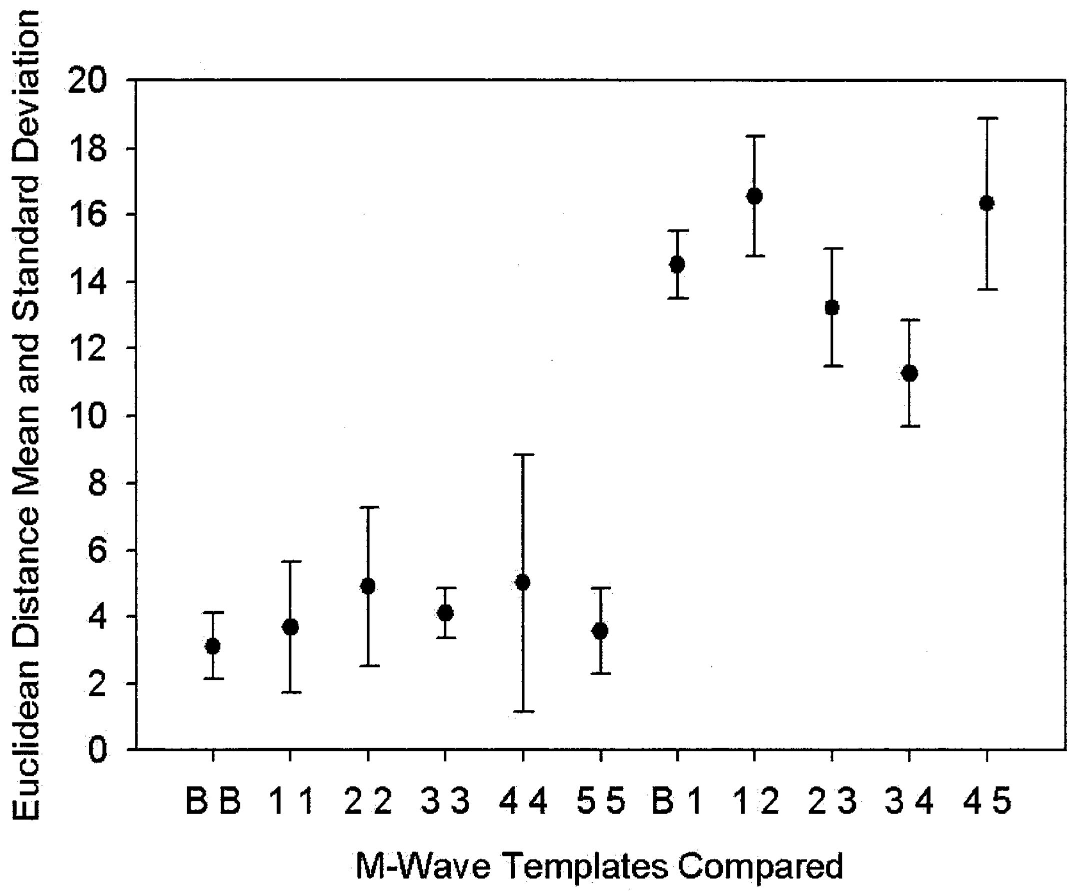

Figure 5.12. Intra-class and inter-class Euclidean distances for the smallest 5 M-wave templates using a Haar mother wavelet for feature extraction

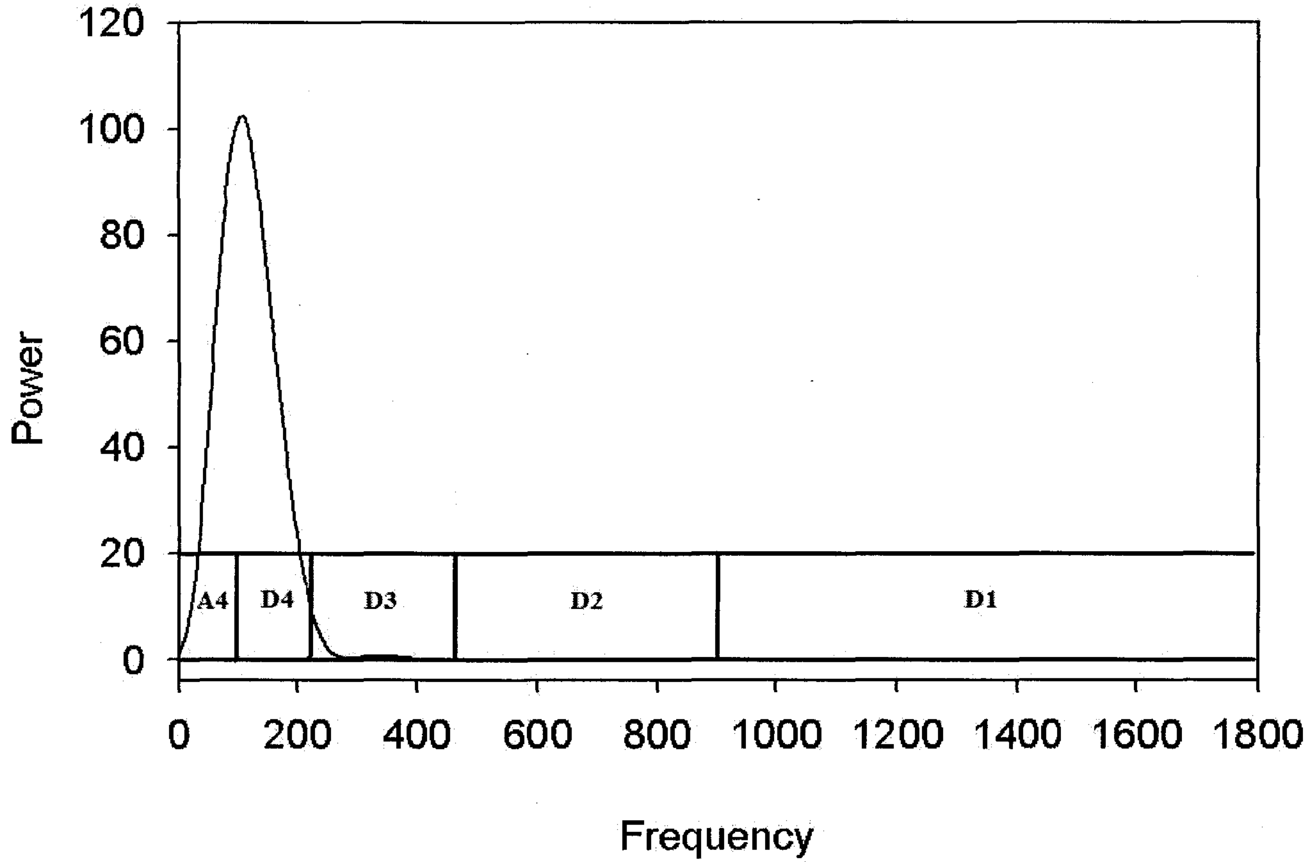

Figure 5.13. Power spectral density for subject B with wavelet decomposition bands

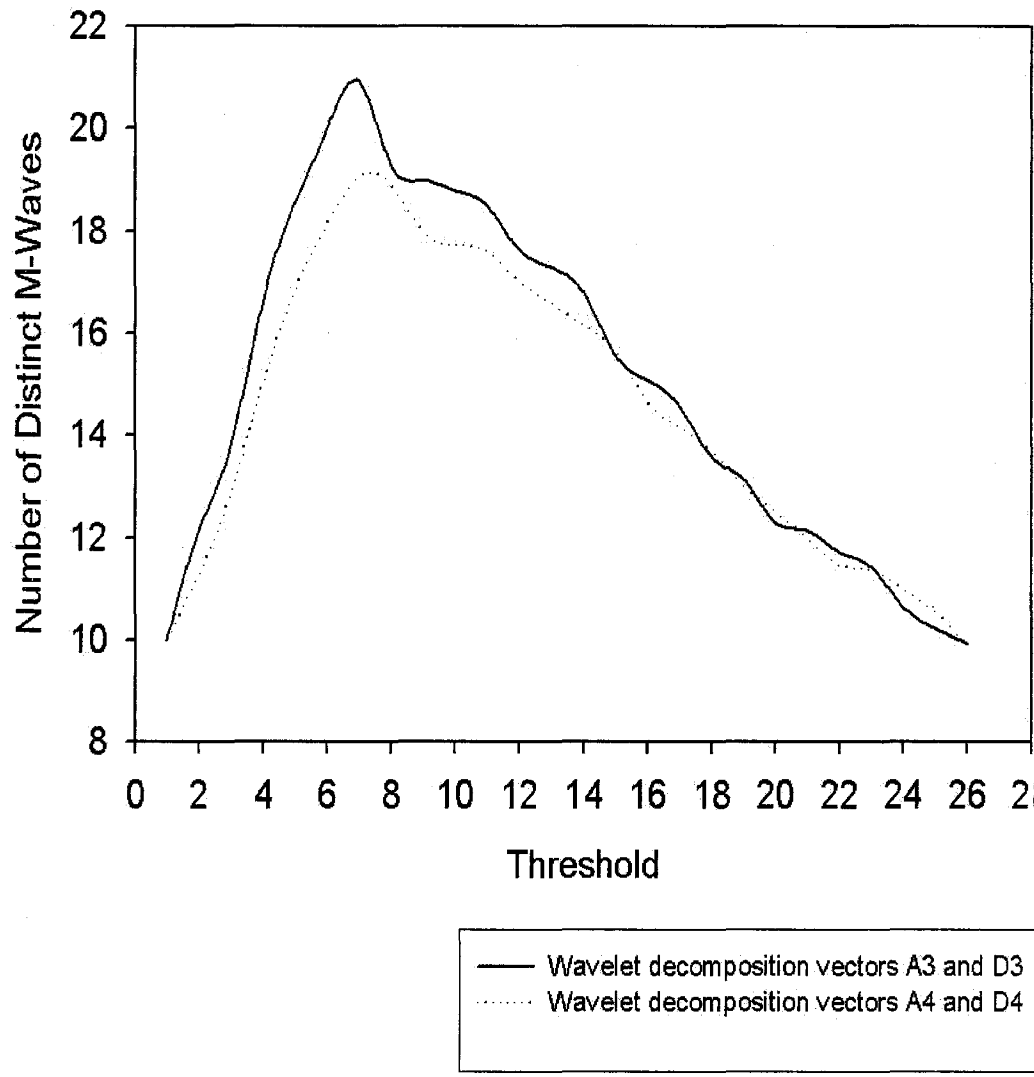

Figure 5.14. Average number of distinct M-waves greater than 10, when using the vectors A3/D3 and A4/D4 for a Daubechies 5 wavelet decomposition

choice of a 3-level decomposition. However, Figure 5.13, which gives the power spectrum for a different subject gives reason to suspect that a 4-level decomposition may offer improved performance. This figure shows that the frequency band in which the M-wave signals have the maximum power can be captured by wavelet vectors a4 and d4. While, the wavelet vector d3 captures some relevant signal information, Figure 5.13 suggests this information may be unnecessary for clustering the M-waves. Figure 5.14 shows the resulting M-wave numbers when the wavelets vectors a4/d4 as opposed to a3/d3 are used as the feature set in a Daubechies 5 wavelet pattern recognition scheme. This figure shows that when the vectors a4 and d4 are used as the features for the classifier to act on, the resulting maximum M-wave number is less. The implication is that the a4/d4 pattern classification scheme fails to differentiate between several clusters of M-waves. Thus, the information captured in the third level detail vector, d3, is relevant for M-wave pattern recognition. Contrarily, for a 3-level decomposition when the vectors d1 and d2 are included in the analysis along with a3 and d3, the resulting M-wave numbers over varying thresholds remain unchanged. This proves that the information contained in the high frequency bands captured by d1 and d2 is not descriptive of the M-wave signal features and thus, may be disregarded in the pattern recognition. High frequency content of larger M-waves probably decreases because of the summation effect of many MUAPs.

5.10 Time Invariant Wavelet

When an electrical stimulus is applied to elicit an evoked response in a muscle, AP generation is most likely to occur at the nodes of Ranvier (see Figure 2.1). The voltage field in the tissue under the stimulating electrodes determines whether the AP will initiate simultaneously at several adjacent nodes of Ranvier. If the AP does initiate at several nodes of Ranvier under the cathode, it is the most distal node that determines the latency between stimulus application and the arrival of the MUAP. When the distal node is hovering around the activation threshold, AP generation may alternate between this node and the adjacent node closer to the cathode on successive stimulations. Therefore, for repetitive stimuli, the resulting M-wave responses may be time-shifted versions of each other. This situation is shown in Figure 5.15.

Latency shifting is an important occurrence to be aware of in pattern recognition. While a fully trained manual operator can recognize time-shifted waveforms as belonging to the same M-wave cluster, automated pattern recognition techniques may not. As discussed in Section 3.5 one of the inherent problems with the wavelet transform is its inability to recognize time-shifted waveforms. Power spectral analysis does not have this problem because the Fourier transform disregards all time information in a signal and is concerned only with the frequency components that exist. Due to wavelets sensitivity to translation, a shift-invariant wavelet transform is more optimal for M-wave pattern recognition than the traditional transform.

The shift-invariant wavelet transform described in Section 3.5 offers a solution for M-wave pattern recognition when latency shifts affect the data. To analyze the effects of

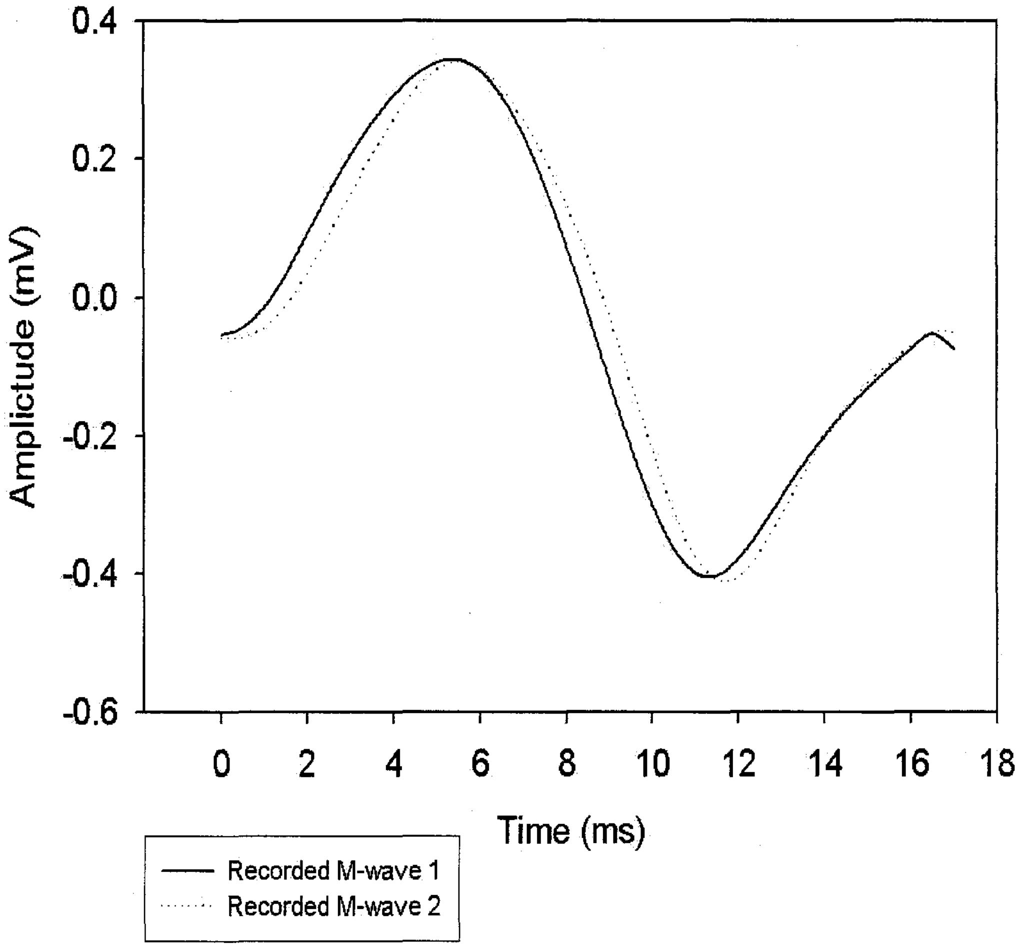

Figure 5.15. Two separately recorded M-waves from 1 subject that are identical except for a time translation

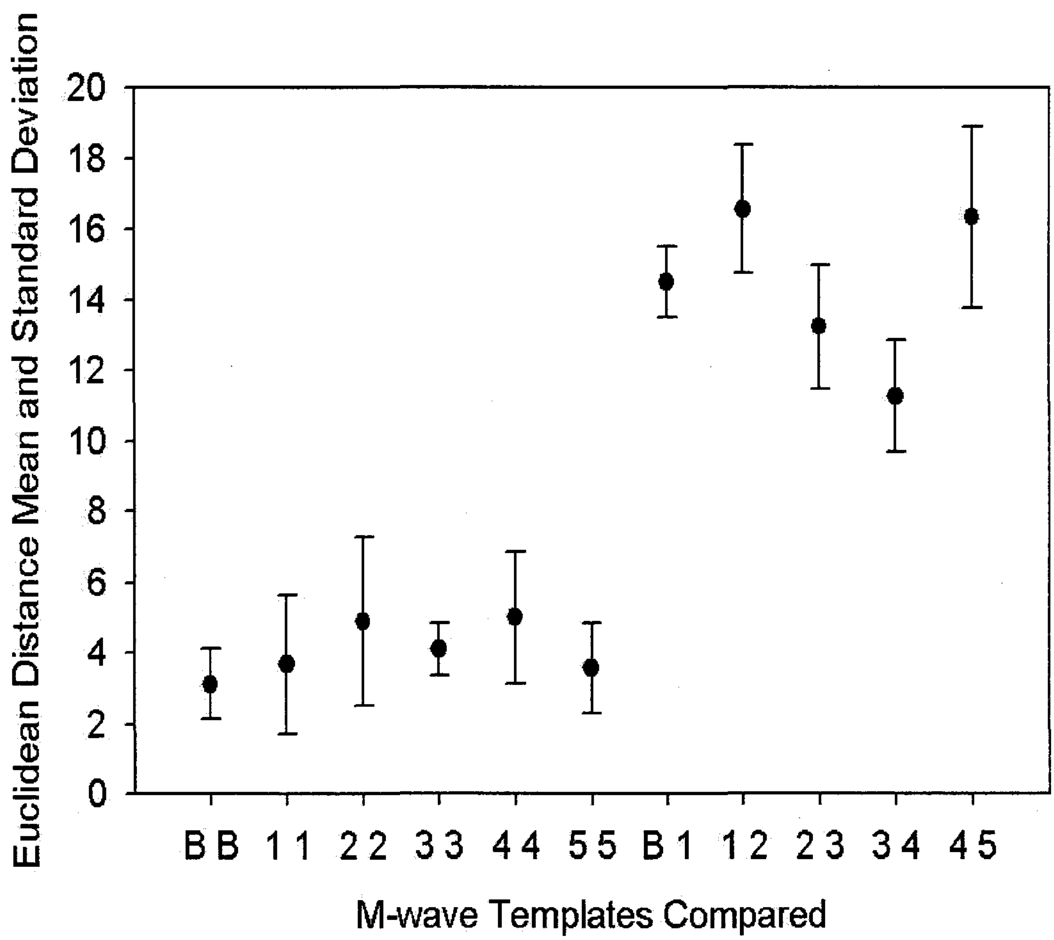

Figure 5.16. Intra-class and inter-class Euclidean distances for the smallest 5 M-wave templates using a shift-invariant wavelet for feature extraction

a shift-invariant wavelet on M-wave pattern recognition, the intra- and inter-class distances for the 1 subject's data were calculated and compared to Figure 5.8. Figure 5.16, shows the intra- and inter-class distances for the time-shifted wavelet based recognition. When compared to Figure 5.9 (B), it is evident that the time-shifted wavelet generates features that are more separable than the traditional wavelet. This makes sense intuitively. When two recorded M-waves are identical but translated, the traditional wavelet transform generates different coefficients for each. Thus, the Euclidean distance calculated between these two M-waves will be large. Depending on the nature of the waveforms and the value of the discriminatory threshold, this Euclidean distance will be an outlier. That is, it will be close to the threshold value and the waveforms may either be classed as the same or different. However, regardless of the class, the Euclidean distance will be largely different from either the intra-, if clustered together, or inter-class, if clustered separately, averages. The standard deviation for both the intra- and inter-class distances will be larger when translation is recognized. Contrarily, the shift-invariant wavelet does not generate largely different coefficients for translated M-waves. The resulting Euclidean distance between two such recordings will be minimal. The shift-invariant wavelet will cluster translated waveforms together and because the Euclidean distance is not an outlier, the standard deviation will be smaller.

It appears then, that a shift-invariant wavelet transform should be employed when extracting features for automatic M-wave pattern recognition. However, the shift-invariant wavelet transform is computationally more involved than the traditional wavelet and its use must therefore provide significant improvements for clustering M-waves.

Further investigation of the shift-invariant wavelet transform was beyond the scope of this thesis.

CHAPTER 6
CONCLUSIONS

6.1 Conclusions

This study investigates the use of different feature sets for M-wave pattern classification. The real-time LabVIEW system developed for this work provides a practical and reliable approach for collecting and recognizing evoked M-wave responses. The computer interface is user-friendly and provides appropriate displays to aid an experienced operator in M-wave collection. Furthermore, the necessary instrumentation is easy to apply and is comfortable for the subject. Additionally, the process is non-invasive and time-efficient so the subject experiences a minimum number of electrical stimuli. This results in less anxiety of the subject and thus, less background EMG during the recording.

Results were obtained from the right and left thenar muscles of 4 healthy females and 2 healthy males. Pattern recognition to determine M-wave templates from the recorded data was performed using various methods to extract features. For all valid extractors, separability between the feature sets of unique M-wave templates must exist. A boundary or threshold between unique M-waves must be determined empirically from a large range of subjects. This universal threshold greatly affects the performance of different feature extractors in M-wave pattern recognition. Analysis of the 6 subjects showed that a universal threshold is one where the average number of unique M-wave templates is a maximum. For the 6 subjects, the average distance between the individual optimal threshold and the universal threshold was 51% of the universal threshold for power spectral based features and 43% of the universal threshold for wavelet features.

This corresponded to a range of M-wave number values from 20% of the average maximum value to the maximum value. It was then determined that the best feature set is that which gives an M-wave number within 20% of the maximum average number over the largest discriminatory threshold range. This feature set would be least sensitive to threshold ranges and thus, provide the most robust pattern recognition scheme.

The 3-level Daubechies 5 wavelet vectors A3 and D3 were found to provide a pattern recognition technique that is less sensitive to threshold changes than a power spectral approach. Furthermore, intra- and inter-class distance measures show power spectral features to be less separable than wavelet features. The choice of mother wavelet and decomposition level largely impacts the success of a wavelet based feature extractor. The Haar mother wavelet was found to generate features that are less separable than those generated by a Daubechies 5 mother wavelet. In addition, for typical M-wave data sets, the wavelet vectors A3 and D3 gave a feature set that led to accurate M-wave numbers while being relatively insensitive to threshold changes. Contrarily, the wavelet vectors A4 and D4 produced feature sets that resulted in low M-wave numbers. Initial analysis with a shift-invariant wavelet feature extractor showed that this tool generates features that are more separable than traditional wavelet features.

Although the virtual instrument developed for this thesis is very flexible and user friendly, the analog instrumentation, cabling and electromagnetic environment were not ideal. This resulted in a high level of additive noise in the recorded responses. A number of noise reduction algorithms were developed that were able to remove most of the noise. The pattern recognition test results were therefore obtained in a "worst case" environment. Since clinical signal acquisition hardware and labs are higher quality as regards to noise, it is safe to conclude that the wavelet pattern recognition scheme should work successfully in the clinical environment. The only remaining source of noise that is not hardware dependent is background EMG. This could possibly be reduced by better supporting the subjects' limbs or having them lie in bed.

6.2 Future Research

Implementation of an advanced alternation algorithm should be examined. Though alternation may always be present due to the nature of the McComas method, techniques to reduce its effects are available and should be included in the real-time LabVIEW program.

Further investigation into the shift-invariant wavelet is warranted. Also the possibility of using a varying threshold in wavelet pattern recognition should be examined.

The present system provides a means for determining unique M-wave templates from recorded evoked responses. With simple modifications this system could be programmed to calculate MUNEs in real-time. This would then allow the system to be used in tracking functional MU populations, both in healthy and diseased individuals. Moreover, the system may be used to monitor and assess motor-neural diseases. Finally, the modified system may also contribute to research purposes by studying the effects of aging on a MU population.

REFERENCES

Ballantyne JP, Hansen S. "A new method for the estimation of the number of motor units in a muscle. 1. Control subjects and patients with myasthenia gravis," Journal of Neurology, Neurosurgery and Psychiatry, 37:907-915, 1974.

Ballantyne JP, Hansen S. "Computer method for the analysis of evoked motor unit potentials. 2. Duchenne, limbgirdle, facioscapulohumeral and myotonic muscular dystrophy," Journal of Neurology, Neurosurgery, and Psychiatry, 38:417-428, 1975.

Cavasin R. An Automated Muscle Motor Unit Counting System, Master's Thesis. Hamilton: McMaster University, 1989.

Chan KM, Doherty TJ, Andres LP, Porter MM, Brown T, Borwn WF. "Longitudinal study of the contractile and electrical properties of single human thenar motor units," Muscle & Nerve, 21:839-849, 1998.

Cooley JW, Tukey JW. "An algorithm for the machine computation of the complex Fourier series," Mathematics of Computation, 19:297-301, 1965.

Daube JR. "MUNE by statistical analysis," Motor Unit Number Estimation (Supplements to Clinical Neurophysiology Vol. 55), 51-71, 2003.

Doherty TJ, Brown WF. "The estimated numbers and relative sizes of thenar motor units as selected by multiple point stimulation in young and older adults," Muscle & Nerve, 16:355-366, 1993.

Doherty TJ,Stashuk DW, Brown WF. "Determinants of mean motor unit size: impact on estimates of motor unit number," Muscle & Nerve, 16:1326-1331, 1993.

Feinstein B, Lindegard B, Nyman E, Wohlfart G. "Morphological studies of motor units in normal human muscles," Acta Anatomica, 23:127-142, 1955.

Gabor D, "Theory of communication," Journal of Institute of Electrical Engineering, 93:429-457, 1946.

Galea V, de Bruin H, Cavasin R, McComas AJ. "The numbers and relative sizes of motor units estimated by computer," Muscle & Nerve, 14:1123-1130, 1991.

Guyton AC, Hall JE. Textbook of Medical Physiology, New York: W.B. Saunders Co.,1996.

Hu X, Wang Z. "Detecting the motor unit action potential from surface EMG signals based on wavelet transform," IEEE International Workshop on Biomedical Circuits & Systems, 2.6-15, 2004.

Jashenko JG. Automatic Estimation of the Number of Muscle Motor Units, Master's Thesis. Hamilton: McMaster University, 1987.

Mallat S. "A theory for multiresolution signal decomposition: the wavelet representation," IEEE Pattern Analysis and Machine Intelligence, 11:674-693, 1989.

McComas AJ, Fawcett PRW, Campbell MJ, and Sica REP. "Electrophysiological estimation of the number of motor units within a human muscle," Journal of Neurology, Neurosurgery and Psychiatry, 34:121-131, 1971.

McComas AJ, Galea V, de Bruin H. "Morot unit populations in healthy and diseased muscles," Physical Therapy, 73:868-877, 1993.

Orsi C. Extraction of Acceleration Signals Related to Motor Unit Action Potentials, Master's Thesis. Hamilton: McMaster University, 2000.

Sari-Sarraf H, Brzakovic D. "A Shift-Invariant Wavelet Transform," IEEE Transactions on Signal Processing, 45:2621-2626, 1997.

Slawnych M, Laszlo C, Hershler C. "Motor unit estimates obtained using the new MUESA method," Muscle & Nerve, 19:626-636, 1996.

Stein RB, Yang JF. "Methods for estimating the number of motor units in human muscles," Annals of Neurology, 28:487-495, 1990.

Szlavik R, de Bruin H. "The effect of stimulus current pulse width on nerve fiber size recruitment patterns," Medical Engineering & Physics, 21:507-515, 1999.

Zhou P, Rymer WZ. "Motor unit action potential number in the surface electromyogram: wavelet matching method and its performance boundary," Proceedings of the 1st International IEEE EMBS Conference on Neural Engineering, 336-339, 2003.